Water Resources Research

TECHNICAL REPORTS: METHODS
10.1029/2020WR027106

Practical and Theoretical Benefits of an Alternative to the Penman-Monteith Evapotranspiration Equation

Kaighin A. McColl[1,2]

[1]Department of Earth and Planetary Sciences, Harvard University, Cambridge, MA, USA, [2]School of Engineering and Applied Sciences, Harvard University, Cambridge, MA, USA

Key Points:
- The Penman-Monteith evapotranspiration equation is incorrect in important limiting cases
- I present an alternative equation that is correct in all limits and more accurate in real-world conditions
- The alternative equation does not require any additional assumptions, empiricism, or computational cost

Supporting Information:
- Supporting Information S1

Correspondence to:
K. A. McColl,
kmccoll@seas.harvard.edu

Citation:
McColl, K. A. (2020). Practical and theoretical benefits of an alternative to the Penman-Monteith evapotranspiration equation. *Water Resources Research*, *56*, e2020WR027106. https://doi.org/10.1029/2020WR027106

Received 10 JAN 2020
Accepted 23 MAR 2020
Accepted article online 15 APR 2020

Abstract The Penman-Monteith equation is used widely to estimate evapotranspiration (E) and to understand its governing physics. I present an alternative to the Penman-Monteith equation that has both practical and theoretical advantages, at no appreciable cost. In particular, the new equation requires no additional assumptions, empiricism, or computational cost compared with the Penman-Monteith equation. Practically, the new equation is consistently more accurate over a wide range of conditions when compared with eddy covariance observations: The new equation has lower errors compared with Penman-Monteith estimates of ET at all of the 79 eddy covariance sites available for the analysis. Using the new equation reduces errors, on average, by 67%, from 8.55 to 2.81 [W m^{-2}]. At night, the improvement is even greater (92% reduction in error; from 1.26 to 0.097 [W m^{-2}]). This improvement is achieved without calibration. Theoretically, the new equation corrects a conceptual error in the Penman-Monteith equation, in which the Penman-Monteith equation incorrectly implies that E from a saturated surface into a saturated, turbulent atmosphere ("equilibrium" E) is *exactly* equivalent to E from an unsaturated surface into an unsaturated, laminar atmosphere. The conceptual error is traced back to the failure of the Penman-Monteith equation in important limiting cases; these errors are eliminated by the new equation. I use the new equation to revise an existing theory of land-atmosphere coupling affected by the conceptual error in the Penman-Monteith equation and to reassess several common but incorrect definitions of equilibrium E.

1. Introduction

Evapotranspiration (E [kg m^{-2} s^{-1}]) is the second largest flux of water, after precipitation, in the terrestrial water cycle. It is a key component of the surface energy budget, in which the difference between net radiation and ground heat flux ($R_n - G$ [W m^{-2}]) balances turbulent fluxes of sensible and latent heat ($H + \lambda E$ [W m^{-2}], where λ is the latent heat of vaporization [J kg^{-1}]). During the daytime, when typically $R_n - G > 0$, E cools and moistens the lower atmosphere. E can also remain significant at night (Dawson et al., 2007; Groh et al., 2019; Novick et al., 2009), when typically $R_n - G < 0$.

E is governed by the surface energy budget,

$$R_n - G = \overbrace{\rho\lambda\frac{g_s g_a}{g_s + g_a}(q^*(T_s) - q_a)}^{\text{Latent heat flux} \quad \lambda E} + \overbrace{\rho c_p g_a (T_s - T_a)}^{\text{Sensible heat flux} \quad H}, \tag{1}$$

where T_s is surface temperature [K], T_a is air temperature at screen-level [K], $q^*(T_s)$ is saturated specific humidity at the surface [—] specified by the Clausius-Clapeyron relation, q_a is specific humidity of air at screen level [—]), ρ is air density [kg m^{-3}], and c_p is the specific heat capacity of air at constant pressure [J kg^{-1} K^{-1}]. E is constrained by water availability and plant physiology, modeled by the bulk parameter g_s [m s^{-1}], often referred to as the "ecosystem conductance." It is also constrained by turbulent transport, modeled by the bulk parameter g_a [m s^{-1}], or "aerodynamic conductance." Equation (1) gives the "radiatively uncoupled" surface energy budget (Raupach, 2001), in which R_n and G are treated as known and do not vary explicitly with surface temperature T_s; this applies, for instance, if direct observations of R_n and G are available. If R_n and G are modeled rather than observed, their dependence on T_s can be retained in the analysis by introducing a "radiative conductance," g_r, and "storage conductance," g_g (the "radiatively coupled" case, considered in Appendix B).

10.1029/2020WR027106

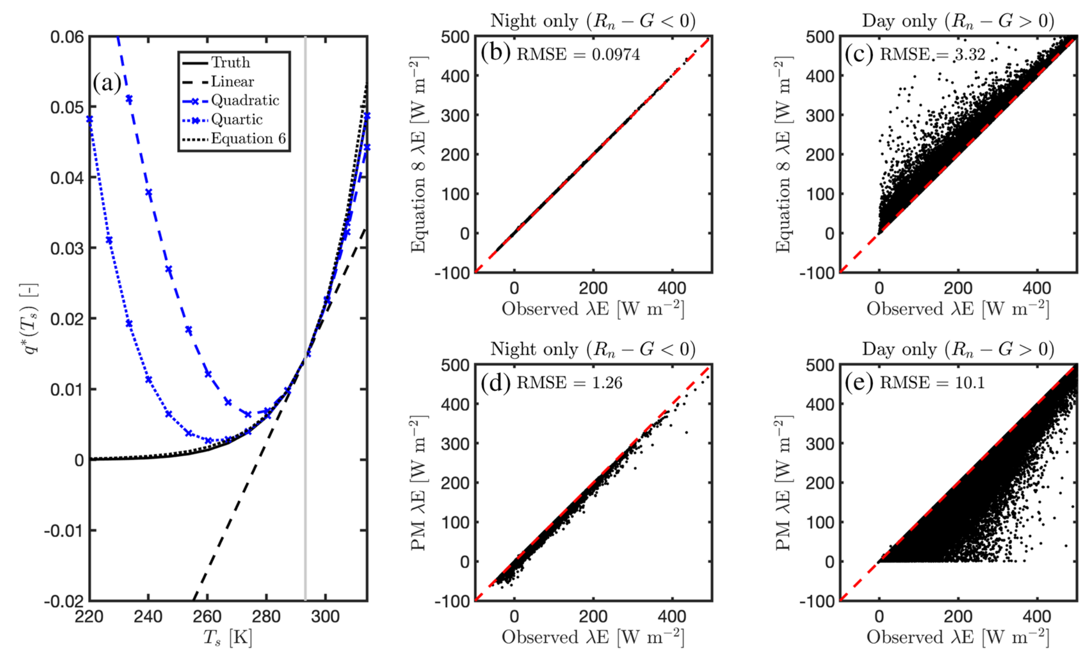

Figure 1. Practical benefits of equation (8): (a) approximations to the Clausius-Clapeyron relation, where $q^*(T_s)$ is the saturated specific humidity [—] and T_s is surface temperature [K]. In this example, the vertical gray line is the air temperature T_a [K] used in each approximation. The linear approximation, used in the PM equation, is a first-order Taylor expansion around $T_s = T_a$. The quadratic and quartic approximations are second- and fourth-order expansions, respectively. Comparison of equation (8) (b, c) and the PM equation (d, e) with half-hourly observations from 79 FLUXNET sites. The red dashed line is the 1:1 line. "PM" means "Penman-Monteith." "RMSE" means "root-mean-squared error."

Given observations or model estimates of R_n, G, q_a, T_a, g_s and g_a, equation (1) is an implicit equation for T_s. Since T_s is present in the definition of E, it is also an implicit equation for E. Equation (1) cannot be solved for T_s analytically, due to the presence of the nonlinear $q^*(T_s)$. An approximate solution can be obtained by linearizing $q^*(T_s)$ around $T = T_a$ (Figure 1), that is,

$$q^*(T_s) \approx q^*(T_a) + \overbrace{\left.\frac{dq^*}{dT}\right|_{T=T_a}}^{\equiv\Delta}(T_s - T_a). \tag{2}$$

Using (i) the definition of H to replace $T_s - T_a$ with $H/(\rho c_p g_a)$, (ii) equation (1) to replace H with $R_n - G - \lambda E$, (iii) substituting the resulting equation into the definition of λE, and (iv) solving for λE yields the explicit equation

$$\lambda E = \frac{\epsilon(R_n - G) + \rho\lambda g_a\overbrace{(q^*(T_a) - q_a)}^{\equiv D}}{\epsilon + 1 + \frac{g_a}{g_s}}, \tag{3}$$

where $\epsilon = \frac{\lambda\Delta}{c_p}$ [—]. This is the radiatively uncoupled Penman-Monteith (PM) equation (Monteith, 1965; Penman, 1948) (see Appendix B for the radiatively coupled version). The major benefit of the PM equation is its removal of explicit dependence on T_s. While the surface energy balance could be solved numerically for T_s and λE, the PM equation provides an approximate but explicit solution that has proven theoretically useful in understanding the coupled land-atmosphere system (e.g., Jarvis & McNaughton, 1986; Konings et al., 2011; Raupach, 2001; Scheff & Frierson, 2013; Stap et al., 2014; van Heerwaarden et al., 2010). It has also been widely applied in estimating E from field data, used within macroscale hydrology models (Hamman et al., 2018; Liang et al., 1994) and land surface models (Kumar et al., 2017) and has been inverted to estimate ecosystem-scale g_s from observations of E and other variables (e.g., Baldocchi et al., 1991; Lin et al., 2018; Novick et al., 2016).

Unfortunately, the linearization of the Clausius-Clapeyron relation in the PM equation introduces both empirical and conceptual errors into estimates of λE. Empirically, the linearization of the Clausius-Clapeyron relation can be quite inaccurate (Milly, 1991; Paw U & Gao, 1988), particularly at night and in cold environments. Conceptually, the PM equation is incorrect in important limiting cases, which has led to common conceptual mistakes in the literature, related to λE under well-watered conditions and other limiting cases (Paw U & Gao, 1988).

To remedy these problems, I propose an alternative to the PM equation—based on an approximation of the Clausius-Clapeyron relation proposed by Vallis et al. (2019)—that substantially reduces its empirical errors and eliminates its conceptual errors. Like the PM equation, the new equation is an explicit solution for λE based on equation (1). Unlike the PM equation, it reproduces the correct limiting behavior, eliminating conceptual errors. Empirically, the new equation is more accurate than the PM equation across a wide range of real-world conditions, at no additional cost in terms of required assumptions, inputs, parameters, empiricism, or computation. Many challenges in modeling ET are not addressed by this work, including the modeling and estimation of g_a and g_s; rather, the focus is on improving the PM equation without introducing additional costs.

This manuscript is structured as follows. In section 2, an alternative to the PM equation is presented. In section 2.1, the alternative equation is shown to outperform the PM equation in a range of real-world cases using eddy covariance observations. Readers who are primarily interested in seeing empirical evidence of the accuracy of the new equation should feel free to skip to this section. In section 2.2, the theoretical benefits of equation (8) are introduced. One benefit is its accuracy in limiting cases, which contrasts with the PM equation; the behavior of both equations in various limiting cases is considered in section 2.3. In section 2.4, the new equation is used to revise an existing theory of land-atmosphere coupling. In light of results in the previous sections, five different definitions of equilibrium E are critically reassessed in section 2.5. Conclusions are presented in section 3. For readers who are interested in immediately using the more accurate radiatively uncoupled equation for E, it is given in equation (8). Code for applying the equation is available from the author's website.

2. An Alternative to the Penman-Monteith Equation

In this section, I introduce the alternative to the PM equation. The new equation is analogous to the PM equation: It uses an approximation of the Clausius-Clapeyron relation to provide an equation for λE that does not have any explicit dependence on T_s. However, compared with the PM equation, I use a much less severe approximation of the Clausius-Clapeyron relation, resulting in a more accurate expression for λE at no additional cost: no extra assumptions, parameters, inputs, or computational expense are required. Several previous studies have used higher-order Taylor expansions of the Clausius-Clapeyron relation (Figure 1a) to derive quadratic and quartic versions of the PM equation that are also more accurate (Baldocchi et al., 2005; Milly, 1991; Paw U & Gao, 1988). While useful in daytime conditions ($R_n - G > 0$), the quadratic and quartic polynomial equations on which these solutions are constructed can be undefined in some cases when $R_n - G < 0$. This work focuses exclusively on general solutions of equation (1), which are defined for all values of $R_n - G$, like the PM equation itself. For notational simplicity, throughout this manuscript, I use the term "daytime" to mean "$R_n - G > 0$" and "nighttime" to mean "$R_n - G < 0$," while recognizing that this is a simplification.

The Clausius-Clapeyron relation can be written as

$$\frac{dq^*(T)}{dT} = \frac{\lambda q^*(T)}{R_v T^2}, \tag{4}$$

where R_v is the gas constant for water vapor [J kg^{-1} K^{-1}]. The relation can be written in terms of q^* rather than saturated vapor pressure e^* [Pa] because these terms are proportional to a very good approximation in Earth's lower atmosphere. While λ is a function of T, its dependence on T is relatively weak under standard atmospheric conditions, and it is conventionally treated as constant. Applying this approximation and integrating equation (4) between the screen-level air temperature T_a and the surface temperature T_s gives

$$q^*(T_s) = q^*(T_a) \exp\left(-\frac{\lambda}{R_v}\left(\frac{1}{T_s} - \frac{1}{T_a}\right)\right). \tag{5}$$

Assuming $T_s - T_a$ is small, as assumed in the PM equation, Vallis et al. (2019) proposed that this could be approximated as

$$q^*(T_s) \approx q^*(T_a)\exp\left(\frac{\lambda}{R_v T_a^2}\left(T_s - T_a\right)\right). \tag{6}$$

Figure 1a compares this approximation to the approximations made in the linear PM equation (equation (2)) and two higher-order approximations. While all approximations are reasonable when $|T_s - T_a|$ is small, equation (6) is much more robust to increases in $|T_s - T_a|$. If the exponential term in equation (6) is linearized around T_a (using the relation $\exp(x) \approx 1 + x$ near $x = 0$), and the Clausius-Clapeyron relation (equation (4)) is substituted in, the resulting expression is identical to equation (2). Therefore, the approximation in equation (6) is already assumed implicitly in the derivation of the PM equation and is not a new assumption.

Substituting equation (6) into the radiatively uncoupled surface energy balance (equation (1)) gives

$$R_n - G = \rho\lambda\frac{g_s g_a}{g_s + g_a}\left(q^*(T_a)\exp\left(\frac{\lambda}{R_v T_a^2}\left(T_s - T_a\right)\right) - q_a\right) + \rho c_p g_a (T_s - T_a). \tag{7}$$

This equation can be solved exactly for T_s; see Appendix A for a derivation of the solution. Substituting this solution into equation (6) and then into the definition of λE, an expression for λE is obtained that has no explicit dependence on T_s, analogous to the PM equation:

$$\lambda E = \frac{\rho c_p g_a W_0\left(\frac{\lambda}{c_p}\frac{\lambda q^*(T_a)}{R_v T_a^2}\frac{g_s}{g_s+g_a}\exp\left(\frac{\lambda}{R_v T_a^2}\frac{R_n - G + \frac{g_s g_a}{g_s+g_a}\rho\lambda q_a}{\rho c_p g_a}\right)\right)}{\lambda/(R_v T_a^2)} - \rho\lambda\frac{g_s g_a}{g_s + g_a}q_a. \tag{8}$$

Equation (8) uses the principal branch of the Lambert W function $W(x)$, an analytic function defined by

$$W(x\exp(x)) = x.$$

$W(x)$ is multivalued for $\frac{-1}{e} \leq x < 0$, with a principal branch $W_0(x)$ and a negative branch $W_{-1}(x)$, and single valued for $x \geq 0$. Since $x \geq 0$ in equation (8), it is safe to restrict our attention to $W_0(x)$ (Figure S1). While less common than other analytic functions (e.g., the natural logarithm, which is defined similarly as $\log(\exp(x)) = x$), the Lambert W function has been used for centuries. $W_0(x)$ is both differentiable ($\frac{dW(x)}{dx} = \frac{W(x)}{x(1+W(x))}$ for $x \neq 0$) and integrable ($\int W(x)dx = x\left(W(x) - 1 + \frac{1}{W(x)}\right) + C$) (Corless et al., 1996). Applications of the Lambert W function in the environmental sciences include an exact expression for the lifting condensation level (Romps, 2017; Yin et al., 2015), a closed-form solution for convective available potential energy (Romps, 2016), a solution for the temperature profile in an idealized model of moist convection (Vallis et al., 2019), a solution of Richards' equation for unsaturated soil water transport (Barry et al., 1993), and various applications in ecology (Lehtonen, 2016).

Equation (8) applies to the radiatively uncoupled surface energy budget. An equivalent equation is derived for the radiatively coupled case in Appendix B.

2.1. Practical Benefits of Equation (8)

In this section, eddy covariance observations are used to assess the accuracy of equation (8) across a wide range of conditions. The performance of equation (8), in terms of root-mean-squared error (RMSE), is shown to be better than that of the PM equation at all sites available for the analysis.

2.1.1. Data

Observations of λE, R_n, G, T_a, wind speed (u [m s^{-1}]), relative humidity ($RH = q_a/q^*(T_a)$ [—]), air pressure (P [Pa]), and friction velocity (u_* [m s^{-1}]) were obtained from the FLUXNET database (fluxnet.ornl.gov). The FLUXNET data set includes half-hourly observations from eddy covariance sites around the world. Sites that did not include all of these observations were excluded. Observations with quality control flags corresponding to poor-quality gapfill were removed. Estimates of vegetation height at each site were obtained from Lin et al. (2018). Both daytime and nighttime observations were used in this analysis. Nighttime observations were filtered using site-specific friction velocity thresholds provided with the FLUXNET database (Barr et al., 2013; Papale et al., 2006). Seventy-nine eddy covariance sites met these requirements and were used in the analysis; information on these data is summarized in Table S1.

The aerodynamic conductance g_a was estimated at each site using the standard relation (Garratt, 1994; Thom & Oliver, 1977)

$$g_a = \frac{k^2 u}{\left(\log\left(\frac{z-d}{z_{0h}}\right) - \Psi_H\right)\left(\log\left(\frac{z-d}{z_{0m}}\right) - \Psi_M\right)}, \tag{9}$$

where $k = 0.41$ is the von Karman constant [—]; z is the measurement height [m]; u is the mean wind speed [m s^{-1}] at height z; $d = \frac{2}{3}h$ is the assumed zero-plane displacement height [m]; h is the vegetation height [m]; z_{0h} and z_{0m} are the thermal and momentum roughness heights [m], respectively (chosen to be $0.01h$ and $0.1h$, respectively, consistent with previous studies (Lin et al., 2018)); and Ψ_M and Ψ_H are the stability correction functions for momentum and heat transfer, respectively [—]. Standard relations are used for Ψ_M and Ψ_H for unstable (Paulson, 1970) and stable conditions (Holtslag & De Bruin, 1988).

For eddy covariance observations, the ecosystem-scale surface conductance g_s is often estimated using a rearranged form of the PM equation (e.g., Lin et al., 2018; Medlyn et al., 2017; Novick et al., 2016; Wullschleger et al., 2002). The aim of this analysis is to quantify errors in this equation, so a different approach is required: instead, the radiatively uncoupled surface energy budget (equation (1)) is solved numerically for g_s at each point in time and space. Specifically, observations of H (estimated as $R_n - G - \lambda E$) and T_a, combined with estimates of g_a, are used to estimate T_s, based on the definition of H in equation (1). The estimated T_s is then combined with observations of λE and q_a to estimate g_s, using the definition of λE in equation (1).

2.1.2. Validation Against Observations

Errors in equation (8) and the PM equation are estimated using observed values of λE, $R_n - G$, T_a, q_a, and estimated values of g_a and g_s, as described in the previous section. Overall, equation (8) consistently outperforms the PM equation. At all 79 sites, compared with the PM equation, equation (8) has lower RMSE with respect to observed λE. Across sites, and using both daytime and nighttime observations, equation (8) results in a 67% reduction in RMSE, reducing it from 8.55 to 2.81 W m^{-2}. At night ($R_n - G < 0$), absolute values of RMSE are lower, since absolute values of λE are lower. However, across sites, the average reduction in RMSE using equation (8) at night is 92%, reducing from 1.26 to 0.0974 W m^{-2} (Figures 1b and 1d). Restricting observations to daytime only ($R_n - G > 0$) results in a reduction in RMSE using equation (8) of 67%, from 10.1 to 3.32 W m^{-2} (Figures 1c and 1e).

The PM equation systematically underestimates λE, whereas equation (8) slightly overestimates it. This behavior can be traced back to the different approximations of the Clausius-Clapeyron relation used in each equation. The linearization of $q^*(T_s)$ used in the derivation of the PM equation (equation (2)) systematically underestimates $q^*(T_s)$ (Figure 1a), causing the PM equation to systematically underestimate λE. In contrast, the approximation of $q^*(T_s)$ used in the derivation of equation (8) (equation (6)) slightly overestimates $q^*(T_s)$ (Figure 1a), causing equation (8) to overestimate λE.

At the half-hourly timescale, the PM equation occasionally performs slightly better than equation (8), but these cases are rare and errors are small. More specifically, for 87% of the half-hourly observations across all sites, equation (8) performs better than the PM equation in terms of RMSE (the RMSE is just the absolute value of one residual at the half-hourly timescale, since there is one observation per half hour). In these cases, the median absolute difference between the half-hourly RMSE for equation (8) and the PM equation is 0.47 [W m^{-2}]; the 95th percentile absolute difference is 10 [W m^{-2}]. For the remaining 13% of half-hourly observations, equation (8) performs slightly worse than the PM equation in terms of RMSE. In these cases, the median absolute difference between the half-hourly RMSE for equation (8) and the PM equation is 0.0061 [W m^{-2}]; the 95th percentile absolute difference is 0.095 [W m^{-2}]. Overall, equation (8) performs better than the PM equation at the half-hourly timescale in a broad majority of cases. When it does not perform better, the difference in performance is very small. When aggregated to longer timescales, the performance of equation (8) is consistently better than that of the PM equation.

These results do not appear to be an artifact of errors in the observations or in the methods used to estimate g_a and g_s from the data. To check this, first, all analyses were repeated using λE estimated as the residual of the observed energy balance at each site, rather than the directly observed value. The results were qualitatively similar (not shown). Second, the equations were also tested on synthetic "observations" (including synthetic observations of g_a and g_s), which are not subject to observation error, or other estimation errors (supporting information Text S1). The results are qualitatively similar to those obtained using real data (Figures S4–S5).

In summary, equation (8) substantially and consistently reduces errors in estimates of λE based on real-world observations, compared with the PM equation. It does so without calibration and without requiring any additional assumptions, inputs, or computational cost.

2.2. Theoretical Benefits of Equation (8)

Important theoretical insights can be gained from analyzing explicit solutions of equation (1), such as the PM equation or equation (8). One major theoretical benefit of an explicit solution over numerically solving equation (1) is that the explicit solution can be differentiated. For example, van Heerwaarden et al. (2010) differentiated the PM equation to analyze forcings and feedbacks in the coupled land-atmosphere system. Another benefit of an explicit solution is that limiting cases—that is, cases in which a governing parameter, such as g_a or g_s, approaches zero or infinity—can be studied analytically. The study of limiting cases of evapotranspiration has a long history (e.g., Paw U & Gao, 1988; Raupach, 2001; Yang & Roderick, 2019). For example, a common example of a limiting case in the study of E is the concept of "potential evapotranspiration": one of many definitions of potential ET is E in the limit of $g_s \to \infty$. Another definition is the case in which, in addition to $g_s \to \infty$, the near-surface air is also saturated. Under this definition, the radiatively uncoupled PM equation converges to the "equilibrium" value,

$$\lambda E \approx \frac{\epsilon}{\epsilon + 1}(R_n - G). \tag{10}$$

Raupach (2001) provides a comprehensive review of equilibrium ET. Conveniently, this relation does not depend on wind speed or surface conditions, including surface temperature (this applies for the radiatively uncoupled case (Raupach, 2001)). The relation has been empirically adapted to the more common case in which the air is unsaturated, by multiplying the equilibrium value by a constant, often taken to be 1.26 (Priestley & Taylor, 1972). This variant of equilibrium ET is at the core of modern ET estimation algorithms, such as the Priestley-Taylor Jet Propulsion Lab (PT-JPL) algorithm (Fisher et al., 2008) used in the ECOsystem Spaceborne Thermal Radiometer Experiment on the Space Station (ECOSTRESS) mission (Stavros et al., 2017); the widely used Global Land Evaporation Amsterdam Model (GLEAM) algorithm (Martens et al., 2017); and a recent theory of land-atmosphere coupling (McColl et al., 2019; McColl & Rigden, 2020).

Given the considerable importance of equilibrium ET and other limiting cases in understanding and modeling ET, any approximate solution of λE based on equation (1) should reproduce the correct limiting behavior. In the following section, I show that, in contrast to equation (8), the PM equation does not reproduce the correct limiting behavior in all cases.

2.3. Limiting Behavior of the PM Equation and Equation (8)

In this section, I compare predictions of λE in several limiting cases based on the PM equation and equation (8), with the true limiting behavior implied by the radiatively uncoupled surface energy budget (equation (1)). The radiatively uncoupled case is of primary interest in this section because, as we will see, two common definitions of equilibrium ET are based on limits of the radiatively uncoupled surface energy budget. I will show that one of these definitions is incorrect.

For readers not familiar with limits, the expression "$\lambda E \to X$ as $g_a \to 0$" can be interpreted as "X is a reasonable approximation of λE when g_a is sufficiently small." The expression "$\lambda E \to X$ as $g_a \to \infty$" can be interpreted as "X is a reasonable approximation of λE when g_a is sufficiently large." When considered this way, a limit has clear practical relevance as a useful approximation in real-world cases.

While various limiting cases of the surface energy budget could be considered, this study focuses exclusively on the limiting cases in which g_a and g_s approach both zero and infinity, consistent with previous studies (Raupach, 2001).

2.3.1. The Wet Limit: $g_s \to \infty$

The wet limit can be a reasonable approximation of E from a saturated surface, such as a lake or saturated soil. We consider two variants of this case: one in which the air is also saturated ($D = 0$ and $g_s \to \infty$) and one in which it is not ($D > 0$ and $g_s \to \infty$).

For the case where $D = 0$, the surface energy budget can be rewritten exactly as

$$\lambda E = \frac{\epsilon_{sa}}{\epsilon_{sa} + 1}(R_n - G), \text{ where } \epsilon_{sa} = \frac{\lambda}{c_p}\frac{q^*(T_s) - q^*(T_a)}{T_s - T_a},$$

which does not contain explicit dependence on g_a. However, there is implicit dependence, since T_s is an implicit function of g_a, and so the limiting value varies with g_a. The PM equation approximates $\epsilon_{sa} \approx \epsilon$, removing all dependence on T_s and thus g_a. While this turns out to be a reasonable approximation in this limit, technically, there is still some dependence on g_a. Equation (8) is a function of g_a in this limit and is numerically more accurate, compared to the PM equation, as shown numerically in Figure S7.

For the case where $D > 0$, the PM equation systematically underestimates the true value in this limit. This result is illustrated numerically using synthetic observations, since there is no closed-form solution to equation (1) in this case. Synthetic "truth" observations are generated by solving equation (1) for λE. To numerically approximate this limiting case, g_s is chosen to be 10^{15} [m s^{-1}] and $RH = 0.5$ [—]. Other parameters are set to the following fixed values: $T_a = 20$ [° C], $P = 101.325$ [Pa], and $G = 0$ [W m^{-2}]. Finally, g_a is randomly varied between 0.01 and 0.1 [m s^{-1}], and R_n is randomly varied between −200 and 500 [W m^{-2}]. The synthetic "truth" observations are then compared with the predicted λE obtained using the PM equation and equation (8) (Figure S2). Equation (8) is numerically more accurate than the PM equation and does not systematically underestimate λE in this limiting case, unlike the PM equation. Similar performance is found if the radiatively coupled surface energy budget and corresponding radiatively coupled versions of the PM equation and equation (8) are used instead (not shown).

2.3.2. The Dry Limit: $g_s \to 0$

The dry limit can be a reasonable approximation of E in an arid environment, where water availability limits E. Physically, λE should be zero, since the surface conductance is limiting. Both the PM equation and equation (8) give the correct limiting behavior: $\lambda E \to 0$ as $g_s \to 0$.

2.3.3. The Rough Limit: $g_a \to \infty$

The rough limit can be a reasonable approximation of E over a rough surface, such as a forest. Physically, the temperature gradient approaches zero ($T_s \to T_a$) to maintain finite sensible heat flux. This implies that $\lambda E = \rho\lambda \frac{g_s}{g_s/g_a+1}(q^*(T_s) - q_a) \to \rho\lambda g_s(q^*(T_a) - q_a)$ as $g_a \to \infty$. Both the PM equation and equation (8) correctly reproduce this limit (see Appendix C for a derivation).

2.3.4. The Calm Limit: $g_a \to 0$

This limit corresponds to a case in which turbulent diffusion becomes small. The radiatively uncoupled PM equation (equation (3)) implies that the calm limit ($g_a \to 0$) is exactly equivalent to the "wet" limit ($g_s \to \infty$ and $D = 0$), with λE converging to the "equilibrium" value (equation (10)) in both cases. It is still common to find references to equilibrium E as the radiatively uncoupled limit in which $g_a \to 0$ (e.g., Jones, 2014; Raupach, 2001). From this, a puzzle arises: For a given observed value of $R_n - G$, why would E from a saturated surface into a saturated, turbulent atmosphere be *exactly* equivalent to E from an unsaturated surface into an unsaturated, laminar atmosphere, in general? If this were true, it would require a deep and fundamental connection between turbulent and laminar processes.

In this section, I show that this apparent equivalence is incorrect. Paw U and Gao (1988) showed the limiting behavior produced by the PM equation for the calm limit is incorrect during daytime conditions, and I extend that analysis here to show that it is also incorrect at night.

The PM equation converges to equilibrium E (equation (10)) in two cases. The first case is a wet limit, in which $g_s \to \infty$ and $D = 0$. This case corresponds to the original definition of equilibrium E, is physically justified, and predates the PM equation. Figure S3 shows two example cases, corresponding to daytime ($R_n - G > 0$, Figure S3b) and nighttime ($R_n - G < 0$, Figure S3d), comparing the solution of the PM equation (equation (3)) to the exact solution obtained from numerically solving the surface energy budget (equation (1)), for different values of g_s. All solutions correctly converge to the equilibrium value as $g_s \to \infty$ when $D = 0$.

The second case is a calm limit, in which $g_a \to 0$. Physically, this limit is approached when there is little atmospheric turbulence (i.e., the atmosphere approaches a laminar state). Diffusion of water vapor from the land surface in the absence of turbulence is slow. This is one of several textbook definitions of equilibrium E (e.g., Jones, 2014), first proposed by Thom (1975). It is derived directly from the PM equation. However, there is no obvious physical reason why this case should be equivalent to the first case. In fact, it is not and is an artifact of the PM equation. To illustrate this, Figures S3a and S3c compare the PM solution to the true solution for different values of g_a, for daytime ($R_n - G > 0$) and nighttime ($R_n - G < 0$) conditions, respectively. As $g_a \to 0$, diffusion of heat and water vapor from the surface becomes very slow and inefficient.

Table 1
Theoretical Benefits of Equation (8): Limiting Behavior of λE and Predicted Limiting Behavior From the PM Equation (λE_{PM}) and Equation (8)

	Radiatively uncoupled	Radiatively coupled
$g_a \to 0$	$\lambda E \to \begin{cases} R_n - G, & \text{for } R_n - G > 0 \\ 0, & \text{for } R_n - G \le 0 \end{cases}$ $\lambda E_{\mathrm{PM}} \to \frac{\epsilon(R_n-G)}{\epsilon+1}$ (incorrect)	$\lambda E \to 0$
$g_a \to \infty$	$\lambda E \to \rho\lambda g_s(q^*(T_a) - q_a)$	$\lambda E \to \rho\lambda g_s(q^*(T_a) - q_a)$
$g_s \to 0$	$\lambda E \to 0$	$\lambda E \to 0$
$g_s \to \infty$	No closed-form solution $\lambda E \approx \frac{\epsilon(R_n-G)}{\epsilon+1}$ when $RH = 1$ λE_{PM} underestimates when $RH < 1$ and $R_n - G < 0$	No closed-form solution λE_{PM} underestimates when $RH < 1$ and $R_n^* - G^* < 0$

Note. True values are given in black text. Equation (8) is correct in all limiting cases (see Appendix C for analytical derivations). Where λE_{PM} incorrectly diverges from the true limit, it is noted with red text.

The land surface is unable to turbulently transport away the incoming energy, and as a result, $|T_s|$ increases substantially. For $R_n - G > 0$, the nonlinear Clausius-Clapeyron relation $q^*(T_s)$ in the definition of λE increases much more rapidly than T_s, the equivalent term in the definition of H. In the limit of $T_s \to \infty$, λE dominates H and consumes all available energy at the surface (Bateni & Entekhabi, 2012; Yang & Roderick, 2019), resulting in the limit $\lambda E \to R_n - G$ as $g_a \to 0$. For $R_n - G < 0$, as $g_a \to 0$, T_s *decreases* substantially, rather than increasing. In this case, T_s decreases much more rapidly than $q^*(T_s)$, which asymptotes to zero; therefore, H dominates λE and consumes all available energy at the surface, resulting in the limit $\lambda E \to 0$ as $g_a \to 0$. In comparison, as $g_a \to 0$, the PM equation incorrectly approaches the equilibrium value, for both positive and negative $R_n - G$.

Why do these artifacts occur? The major assumption behind the PM equation is that a linear approximation of the Clausius-Clapeyron relation (equation (2)) is accurate. This approximation is reasonable when $|T_s - T_a|$ is small but can be extremely inaccurate when this assumption is violated. Figure 1a gives an illustration of this. For small $|T_s - T_a|$, the linear approximation used in the PM equation is quite accurate. However, as the difference between T_s and T_a grows, the accuracy of the linear approximation (and even higher-order quadratic and quartic approximations) degrades. In particular, for the case where $T_s \ll T_a$, none of the linear, quadratic, or quartic approximations approach the correct limiting value of $q^*(T_s) \to 0$; in fact, errors in the higher-order quadratic and quartic approximations grow more rapidly than those for the linear approximation. Since $|T_s - T_a|$ grows very large in the calm limit, this suggests that the PM equation should fail to reproduce the correct limiting behavior.

2.3.5. Summary

In summary, the apparent equivalence between E in the radiatively uncoupled calm ($g_a \to 0$) and wet ($g_s \to \infty$ and $D = 0$) limits is purely an artifact of the PM equation. A major theoretical advantage of equation (8) is that it avoids this problem: In particular, Figure S3 shows that, unlike the PM equation, equation (8) correctly predicts that $\lambda E \to R_n - G$ as $g_a \to 0$ when $R_n - G > 0$ and that $\lambda E \to 0$ when $R_n - G < 0$. It also reproduces the correct limiting behavior when $g_a \to \infty$, $g_s \to 0$, and $g_s \to \infty$. The correct limiting behavior for each case is summarized in Table 1, and inaccurate limits in the PM equation are highlighted in red. It is shown analytically in Appendix C that equation (8) converges to the correct limits in each case.

2.4. A Revised Decoupling Parameter

By correctly representing limiting behavior, equation (8) can be used to correct a conceptual mistake in a theory of land-atmosphere coupling. Jarvis and McNaughton (1986) argued that λE could be scaled between two limiting cases: an "equilibrium" case, in which the atmospheric state was set by the evaporating surface, and an "imposed" case, in which the atmospheric state was independent of the evaporating surface. To quantify this scaling, they proposed a "decoupling parameter" Ω, defined as

$$\lambda E = \Omega \lambda E_{\mathrm{eq}} + (1 - \Omega)\lambda E_{\mathrm{imp}} \tag{11}$$

or equivalently as

$$\Omega = \frac{\lambda E - \lambda E_{\text{imp}}}{\lambda E_{\text{eq}} - \lambda E_{\text{imp}}}, \tag{12}$$

where λE_{eq} is equilibrium latent heat flux and λE_{imp} is the latent heat flux in the limit of $g_a \to \infty$. Based on this definition, they proposed, using the PM equation, that Ω could be estimated as

$$\hat{\Omega} = \frac{\epsilon + 1}{\epsilon + 1 + \frac{g_a}{g_s}}. \tag{13}$$

According to this definition, $\Omega \to 1$ (and, therefore, $\lambda E \to \lambda E_{\text{eq}}$) when $g_s \to \infty$ or when $g_a \to 0$. As shown previously, the latter case is an artifact of the PM equation and is incorrect (Paw U & Gao, 1988).

Using equation (8), this problem can be resolved. I define λE_{eq} as the latent heat flux in the wet limit ($g_s \to \infty$ and $D = 0$) in equation (8). λE_{imp} is defined as the latent heat flux in the rough limit ($g_a \to \infty$), the definition given by Jarvis and McNaughton (1986), in equation (8). Equation (8) is correct in both limiting cases, unlike the PM equation. Substituting these expressions along with equation (8) into equation (12) gives the following estimate:

$$\hat{\Omega} = \frac{g_s\lambda^2((g_a+g_s)q^*(T_a)-g_sq_a)-c_pg_a(g_a+g_s)R_vT_a^2W_0\left(\frac{\lambda}{c_p}\frac{\lambda q^*(T_a)}{R_vT_a^2}\frac{g_s}{g_s+g_a}\exp\left(\frac{\lambda}{R_vT_a^2}\frac{R_n-G+\frac{g_sg_a}{g_s+g_a}\rho\lambda q_a}{\rho c_pg_a}\right)\right)}{(g_a+g_s)\left(\lambda^2((g_a+g_s)q^*(T_a)-g_sq_a)-c_pg_aR_vT_a^2W_0\left(\frac{\lambda}{c_p}\frac{\lambda q^*(T_a)}{R_vT_a^2}\exp\left(\frac{\lambda}{R_vT_a^2}\frac{R_n-G+\rho\lambda g_aq^*(T_a)}{\rho c_pg_a}\right)\right)\right)}. \tag{14}$$

While complicated, this expression does not require any additional information or assumptions beyond those made already by Jarvis and McNaughton (1986). As $g_a \to 0$, both λE and λE_{eq} approach $R_n - G$; therefore, $\hat{\Omega} \to 1$, by equation (12), as for the formulation of Jarvis and McNaughton (1986). The key difference is, in the new formulation, λE_{eq} goes to the correct limit ($R_n - G$) as $g_a \to 0$. This remedies a significant conceptual weakness in the theory.

This discussion has been focused on the radiatively uncoupled case, since this case is most relevant to previous definitions of equilibrium E (equilibrium E is not a limiting value in the radiatively coupled case) and has also been used most widely (e.g., Fisher et al., 2009; De Kauwe et al., 2017). The behavior of the decoupling parameter is different in the radiatively coupled case (Paw U & Gao, 1988), and the decoupling parameter framework has since been generalized to the radiatively coupled case (Martin, 1989; McNaughton & Jarvis, 1991). I provide a derivation of a radiatively coupled equivalent expression to equation (14) in Appendix B.1.

2.5. Revisiting Equilibrium E

In this section, I critically reexamine previous definitions of equilibrium E in light of the presented results. This work implies that several conventional definitions of equilibrium E are incorrect (i.e., are not equivalent to, or even approximations of, equation (10)). Raupach (2001) provides a comprehensive review of equilibrium E, listing five different definitions prevalent in the literature. Here, I critically reassess these definitions, finding that two definitions are clearly incorrect, one is probably incorrect, one is probably correct, and one is correct when considered to be a useful approximation. The definitions are as follows:

- E in the limit of $g_a \to 0$: This is incorrect, as discussed in previous sections.
- E in the limit of complete decoupling ($\Omega = 1$): This definition is also based on the PM equation and is also incorrect (Paw U & Gao, 1988). Even if $\hat{\Omega}$ is appropriately redefined, as in equation (14), $\hat{\Omega} = 1$ does not imply equilibrium E. For example, in the radiatively uncoupled case given above, $\hat{\Omega} \to 1$ as $g_a \to 0$, but λE does not go to the equilibrium value.
- E that is independent of g_a: This relation, proposed by Monteith (1965) and Thom (1975), was obtained by differentiating the PM equation with respect to g_a, setting the resulting expression to zero, and rearranging to solve for λE. While equation (8) is differentiable, the same procedure does not yield a closed-form expression when applied to equation (8). Furthermore, it is not clear when a minimum exists in λE for finite g_a, in general: For example, one exists in Figure S3c but not Figure S3a. It therefore seems likely that this definition is also an incorrect artifact of the PM equation.
- E of a closed system forced with incoming energy and allowed to evolve over a sufficiently long period of time: Previous studies that established this relation used either the PM equation explicitly (Raupach, 2001) or other relations based on the linearization of the Clausius-Clapeyron relation (McNaughton,

1976a, 1976b; Slatyer & McIlroy, 1961). This provides some cause for concern. However, since the results of these studies hold for any value of g_a and g_s, and problems with the PM equation mainly arise in limiting cases, this suggests that the definition and results of these studies are likely to be broadly correct. However, the problem requires further consideration, which is left to future work.

- E in the limit of $g_s \to \infty$ and $D = 0$: This definition is exactly correct when ϵ_{sa} is used in the definition of equilibrium E (Raupach, 2001). When ϵ is used instead, it is typically an accurate approximation over wet surfaces (Milly, 1991).

3. Summary and Conclusions

This study has introduced an alternative to the PM evapotranspiration equation (equation (8)), based on an approximation of the Clausius-Clapeyron relation proposed by Vallis et al. (2019). The new equation has both practical and theoretical benefits over the PM equation. These benefits are obtained without requiring additional assumptions, empiricism, inputs, or computational cost.

Practically, the new equation is consistently more accurate than the PM equation, when validated against eddy covariance observations from 79 sites around the world. More specifically, it reduces RMSEs by 5.74 [W m^{-2}], when averaged over both day and night. Many challenges related to the practical modeling of ET are not addressed by this work, including the modeling and estimation of g_a and g_s.

Theoretically, the PM equation is shown to be incorrect in several important limiting cases, which has led to incorrect definitions of equilibrium E: In particular, the definition of equilibrium E as the limiting value of E in the radiatively uncoupled surface energy budget as $g_a \to 0$, which is an incorrect artifact of the PM equation. The new equation does not suffer from this problem. I use the new relation to show that several other common definitions of equilibrium E are incorrect and to remedy a related conceptual error in the decoupling parameter theory of Jarvis and McNaughton (1986).

Beyond the practical and theoretical applications considered here, this work opens up opportunities for more accurately studying the surface energy budget at night, and in cold environments, where the PM equation is particularly inaccurate.

Appendix A: Derivation of Equation (8)

In this section, I solve equation (7) for T_s and obtain equation (8). Equation (7) can be rearranged to the form

$$p^{T_s} = aT_s + b, \tag{A1}$$

where

$$p \equiv \exp\left(\frac{\lambda}{R_v T_a^2}\right), \tag{A2}$$

$$a \equiv -\frac{c_p \exp\left(\frac{\lambda}{R_v T_a}\right)}{\frac{g_s}{g_s+g_a}\lambda q^*(T_a)}, \tag{A3}$$

$$b \equiv \frac{c_p \exp\left(\frac{\lambda}{R_v T_a}\right)}{\frac{g_s}{g_s+g_a}\lambda q^*(T_a)}\left(\frac{R_n - G + \rho\lambda\frac{g_s g_a}{g_s+g_a}q_a}{\rho c_p g_a}\right). \tag{A4}$$

Defining $-t = T_s + \frac{b}{a}$ converts equation (A1) to $tp^t = -\frac{1}{a}p^{-b/a}$. Based on the definition of the Lambert W function (equation (2)), this gives

$$t = \frac{W_0\left(-\frac{1}{a}p^{-b/a}\log(p)\right)}{\log(p)}$$
$$\to T_s = -\frac{W_0\left(-\frac{1}{a}p^{-b/a}\log(p)\right)}{\log(p)} - \frac{b}{a}.$$

Substituting in equations (A2, A3, A4) yields

$$T_s = T_a + \frac{R_n - G + \rho\lambda \frac{g_s g_a}{g_s+g_a} q_a}{\rho c_p g_a} - \frac{W_0\left(\frac{\lambda}{c_p}\frac{\lambda q^*(T_a)}{R_v T_a^2}\frac{g_s}{g_s+g_a}\exp\left(\frac{\lambda}{R_v T_a^2}\frac{R_n - G + \frac{g_s g_a}{g_s+g_a}\rho\lambda q_a}{\rho c_p g_a}\right)\right)}{\lambda/(R_v T_a^2)}. \tag{A5}$$

By the surface energy balance (equation (1)), $\lambda E = R_n - G - \rho c_p g_a (T_s - T_a)$. Substituting equation (A5) into this yields equation (8).

Appendix B: Generalization to the Radiatively Coupled Surface Energy Budget

The "radiatively coupled" surface energy budget (Raupach, 2001) can be written as

$$\overbrace{(1-a_s)R_{s\downarrow} + e_s(R_{L\downarrow} - \sigma T_s^4)}^{\text{Net radiation} \quad R_n(T_s)} - \overbrace{k_g \frac{T_s - T_g}{d_g}}^{\text{Ground heat flux} \quad G(T_s)} = \overbrace{\rho\lambda\frac{g_s g_a}{g_s + g_a}(q^*(T_s) - q_a)}^{\text{Latent heat flux} \quad \lambda E(T_s)} + \overbrace{\rho c_p g_a (T_s - T_a)}^{\text{Sensible heat flux} \quad H(T_s)}, \tag{B1}$$

where a_s is surface albedo [—], $R_{s\downarrow}$ is downwelling shortwave radiation [W m^{-2}], $R_{L\downarrow}$ is downwelling longwave radiation [W m^{-2}], e_s is surface emissivity [—], σ is the Stefan-Boltzmann constant [W m^{-2} K^{-4}], k_g is soil storage thermal conductivity [W m^{-1} K^{-1}], and d_g a soil storage length scale [m]. This can be rewritten to remove all T_s dependence from the left-hand side:

$$\overbrace{(1-a_s)R_{s\downarrow} + e_s(R_{L\downarrow} - \sigma T_a^4)}^{R_n^*} - \overbrace{k_g \frac{T_a - T_g}{d_g}}^{G^*} = \rho\lambda\frac{g_s g_a}{g_s + g_a}(q^*(T_s) - q_a) + \rho c_p (g_a + g_r + g_g)(T_s - T_a), \tag{B2}$$

where $g_g = k_g/(\rho c_p d_g)$ is the storage conductance and $g_r = e_s \sigma (T_s^4 - T_a^4)/(\rho c_p (T_s - T_a))$ is the radiative conductance. The point of this transformation is to move all the unknowns (in this case, just T_s) to the right-hand side. The left-hand side is treated as a known constant. For the special case $g_r = g_g = 0$ (i.e., ignoring effects of radiative and storage coupling, as is common, such that R_n and G are taken as fixed observations), this reduces to the radiatively uncoupled expression for the surface energy balance (equation (1)).

For the radiatively coupled surface energy budget, substituting equation (2) into equation (B2) and solving gives the following approximate solution for λE:

$$\lambda E = \frac{p\epsilon (R_n^* - G^*) + \rho\lambda g_a (q^*(T_a) - q_a)}{p\epsilon + 1 + \frac{g_a}{g_s}}, \tag{B3}$$

where $p = g_a/(g_a + g_r + g_g)$. This is the radiatively coupled PM equation and reduces to the radiatively uncoupled PM equation for the case where $g_r = g_g = 0$, as expected.

The solution for the radiatively uncoupled surface energy budget (equation (1)) presented in Appendix A is generalized here to the radiatively coupled budget (equation (B2)). Substituting equation (6) into equation (B2) and solving for T_s as in Appendix A

$$T_s = T_a + \frac{R_n^* - G^* + \rho\lambda \frac{g_s g_a}{g_s+g_a} q_a}{\rho c_p g_a / p} - \frac{W_0\left(\frac{\lambda}{c_p}\frac{\lambda q^*(T_a)}{R_v T_a^2}\frac{p g_s}{g_s+g_a}\exp\left(\frac{\lambda}{R_v T_a^2}\frac{R_n^* - G^* + \frac{g_s g_a}{g_s+g_a}\rho\lambda q_a}{\rho c_p g_a / p}\right)\right)}{\lambda/(R_v T_a^2)}. \tag{B4}$$

This expression reduces to equation (A5) when $g_g = g_r = 0$, as expected. By the radiatively coupled surface energy budget (equation (B2)), $\lambda E = R_n^* - G^* - \frac{\rho c_p g_a}{p}(T_s - T_a)$. Substituting equation (B4) into this yields

$$\lambda E = \frac{\frac{\rho c_p g_a}{p} W_0\left(\frac{\lambda}{c_p}\frac{\lambda q^*(T_a)}{R_v T_a^2}\frac{p g_s}{g_s+g_a}\exp\left(\frac{\lambda}{R_v T_a^2}\frac{R_n^* - G^* + \frac{g_s g_a}{g_s+g_a}\rho\lambda q_a}{\rho c_p g_a / p}\right)\right)}{\lambda/(R_v T_a^2)} - \rho\lambda\frac{g_s g_a}{g_s + g_a} q_a. \tag{B5}$$

This expression reduces to equation (8) when $g_g = g_r = 0$, as expected.

Figure S3 is reproduced for the radiatively coupled case in Figure S6. For $R_n^* - G^* > 0$, the limiting behavior for g_s is similar, although the limit as $g_s \to \infty$ is $\frac{\lambda E}{R_n^* - G^*} \to \frac{p\epsilon}{p\epsilon+1} \leq \frac{\epsilon}{\epsilon+1}$ (Figure S6b, Raupach, 2001). The limiting behavior as $g_a \to 0$ is quite different for the radiatively coupled case. This is because, in the calm limit of the radiatively coupled case, T_s remains finite, with outgoing longwave radiation balancing incoming radiation, and consequently, H and λE both approach zero (Figure S6a). Equation (B5) is accurate in all cases.

B.1. Decoupling Parameter

For the radiatively coupled case, the decoupling parameter is given by

$$\hat{\Omega} = \frac{g_s\lambda^2((g_a+g_s)q^*(T_a) - g_s q_a) - \frac{c_p g_a (g_a+g_s) R_v T_a^2}{p} W_0\left(\frac{\lambda}{c_p}\frac{\lambda q^*(T_a)}{R_v T_a^2}\frac{p g_s}{g_s+g_a}\exp\left(p\frac{\lambda}{R_v T_a^2}\frac{R_n^* - G^* + \frac{g_s g_a}{g_s+g_a}\rho\lambda q_a}{\rho c_p g_a}\right)\right)}{(g_a+g_s)\left(\lambda^2((g_a+g_s)q^*(T_a) - g_s q_a) - \frac{c_p g_a R_v T_a^2}{p} W_0\left(\frac{\lambda}{c_p}\frac{\lambda q^*(T_a)}{R_v T_a^2} p\exp\left(p\frac{\lambda}{R_v T_a^2}\frac{R_n^* - G^* + \rho\lambda g_a q^*(T_a)}{\rho c_p g_a}\right)\right)\right)}. \quad \text{(B6)}$$

Based on a similar derivation to that in Appendix C for the limiting behavior of λE, it can be shown that, as $g_a \to 0$, $\hat{\Omega} \to 1$ and $\lambda E \to 0$.

Appendix C: Limiting Behavior of Equation (8) in the Limits $g_s \to \infty$, $g_s \to 0$, $g_a \to \infty$, and $g_a \to 0$

Raupach (2001) comprehensively characterizes the limiting behavior of both the radiatively coupled and radiatively uncoupled PM equation. In this section, I characterize the limiting behavior of equation (8) in both radiatively coupled and radiatively uncoupled cases.

C.1. $g_s \to \infty$ and $D = 0$

In this case, for both the radiatively uncoupled and radiatively coupled cases,

$$\lambda E = \frac{\frac{\rho c_p g_a}{p} W_0\left(\frac{\lambda}{c_p}\frac{\lambda q^*(T_a)}{R_v T_a^2} p\exp\left(\frac{\lambda}{R_v T_a^2}\frac{R_n^* - G^* + g_a\rho\lambda q^*(T_a)}{\rho c_p g_a/p}\right)\right)}{\lambda/(R_v T_a^2)} - \rho\lambda g_s q^*(T_a),$$

where $p = 1$ gives the expression for the radiatively uncoupled case, and $0 \leq p < 1$ describes the radiatively coupled case.

Simulations conducted in this limit (Figure S7) demonstrate that, while the assumed form in PM gives a reasonable first-order estimate, it is entirely insensitive to variability due to varying g_a, as expected. In contrast, equation (8) is more accurate and captures reasonably the sensitivity of λE to variation in g_a, even in the limit of $g_s \to \infty$ and $D = 0$.

C.2. $g_s \to 0$

For both the radiatively uncoupled and radiatively coupled cases, $\lambda E \to 0$, since $W_0(0) = 0$.

C.3. $g_a \to \infty$

C.3.1. Radiatively Uncoupled Case

As $x \to 0$, $W_0(x) \sim x$. In addition, $\frac{g_s g_a}{g_s+g_a} = \frac{g_s}{g_s/g_a+1} \to g_s$ as $g_a \to \infty$. These results will be used in this section.

As $g_a \to \infty$, equation (8) goes to

$$\begin{aligned}\lambda E &\to \frac{\rho c_p g_a\left(\frac{\lambda}{c_p}\frac{\lambda q^*(T_a)}{R_v T_a^2}\frac{g_s}{g_s+g_a}\exp\left(\frac{\lambda}{R_v T_a^2}\frac{R_n - G + \frac{g_s g_a}{g_s+g_a}\rho\lambda q_a}{\rho c_p g_a}\right)\right)}{\lambda/(R_v T_a^2)} - \rho\lambda\frac{g_s g_a}{g_s+g_a}q_a \\ &\to \frac{\rho c_p \frac{\lambda}{c_p}\frac{\lambda q^*(T_a)}{R_v T_a^2} g_s \exp(0)}{\lambda/(R_v T_a^2)} - \rho\lambda g_s q_a \\ &= \rho\lambda g_s(q^*(T_a) - q_a).\end{aligned}$$

C.3.2. Radiatively Coupled Case

As $g_a \to \infty$, $p \to 1$, and so the radiatively coupled case is identical to the radiatively uncoupled case.

C.4. $g_a \to 0$

C.4.1. Radiatively Uncoupled Case

In the limit $x \to \infty$, $W_0(x) = \log(x) - \log(\log(x)) + o(1)$. This result is applied in this derivation.

As $g_a \to 0$, equation (8) goes to

$$\lambda E \to 0 + \frac{\rho c_p g_a}{\frac{\lambda}{R_v T_a^2}} \left(\overbrace{\frac{\lambda}{R_v T_a^2} \frac{R_n - G}{\rho c_p g_a}}^{\text{Term I}} + \overbrace{\log\left(\frac{g_s}{g_s + g_a} \frac{\lambda}{c_p} \frac{\lambda q^*(T_a)}{R_v T_a^2} \exp\left(\frac{g_s}{g_s + g_a} \frac{\lambda}{c_p} \frac{\lambda q^*(T_a)}{R_v T_a^2} \right) \right)}^{\text{Term II}} \right.$$
$$\left. \underbrace{- \log\left(\frac{\lambda}{R_v T_a^2} \frac{R_n - G}{\rho c_p g_a} + \log\left(\frac{g_s}{g_s + g_a} \frac{\lambda}{c_p} \frac{\lambda q^*(T_a)}{R_v T_a^2} \exp\left(\frac{g_s}{g_s + g_a} \frac{\lambda}{c_p} \frac{\lambda q^*(T_a)}{R_v T_a^2} \right) \right) \right)}_{\text{Term III}} + \underbrace{o(1)}_{\text{Term IV}} \right).$$

Evaluating the limits term by term gives

$$\lim_{g_a \to 0} \text{Term I} = \lim_{g_a \to 0} \frac{\rho c_p g_a}{\frac{\lambda}{R_v T_a^2}} \frac{\lambda}{R_v T_a^2} \frac{R_n - G}{\rho c_p g_a} = R_n - G$$

$$\lim_{g_a \to 0} \text{Term II} = \lim_{g_a \to 0} \frac{\rho c_p g_a}{\frac{\lambda}{R_v T_a^2}} \log\left(\frac{g_s}{g_s + g_a} \frac{\lambda}{c_p} \frac{\lambda q^*(T_a)}{R_v T_a^2} \exp\left(\frac{g_s}{g_s + g_a} \frac{\lambda}{c_p} \frac{\lambda q^*(T_a)}{R_v T_a^2} \right) \right) = 0$$

$$\lim_{g_a \to 0} \text{Term III} = \lim_{g_a \to 0} \frac{\rho c_p g_a}{\frac{\lambda}{R_v T_a^2}} \log\left(\frac{\lambda}{R_v T_a^2} \frac{R_n - G}{\rho c_p g_a} + \log\left(\frac{g_s}{g_s + g_a} \frac{\lambda}{c_p} \frac{\lambda q^*(T_a)}{R_v T_a^2} \exp\left(\frac{g_s}{g_s + g_a} \frac{\lambda}{c_p} \frac{\lambda q^*(T_a)}{R_v T_a^2} \right) \right) \right)$$
$$= \lim_{g_a \to 0} \frac{\frac{\rho c_p}{\frac{\lambda}{R_v T_a^2}} \log\left(\frac{\lambda}{R_v T_a^2} \frac{R_n - G}{\rho c_p g_a} + \log\left(\frac{g_s}{g_s + g_a} \frac{\lambda}{c_p} \frac{\lambda q^*(T_a)}{R_v T_a^2} \exp\left(\frac{g_s}{g_s + g_a} \frac{\lambda}{c_p} \frac{\lambda q^*(T_a)}{R_v T_a^2} \right) \right) \right)}{1/g_a}.$$

Since both the numerator and the denominator diverge to infinity as $g_a \to 0$, L'Hôpital's rule is used to evaluate the limit. Differentiating the numerator and the denominator and simplifying give

$$\lim_{g_a \to 0} \text{Term III} = \frac{\rho c_p g_a (\lambda(R_n - G) + \rho (\frac{g_a}{g_s + g_a})^2 (g_s \lambda^2 q^*(T_a) + c_p (g_a + g_s) R_v T_a^2)}{\frac{\lambda}{R_v T_a^2} (\lambda(R_n - G) + \rho c_p g_a R_v T_a^2 \log(\frac{\lambda}{c_p} \frac{\lambda q^*(T_a)}{R_v T_a^2} \frac{g_s}{g_s + g_a} \exp(\frac{\lambda}{c_p} \frac{\lambda q^*(T_a)}{R_v T_a^2} \frac{g_s}{g_s + g_a})))} = 0.$$

Finally,

$$\lim_{g_a \to 0} \text{Term IV} = \frac{\rho c_p g_a}{\frac{\lambda}{R_v T_a^2}} o(1) = 0.$$

Combining these results gives

$$\lim_{g_a \to 0} \lambda E = R_n - G.$$

C.4.2. Radiatively Coupled Case

As $g_a \to 0$, $p \to 0$ and $g_a/p \to g_g + g_r$. Therefore, equation (B5) goes to

$$\lambda E \to \frac{\frac{\rho c_p g_a}{p} W_0\left(\frac{\lambda}{c_p} \frac{\lambda q^*(T_a)}{R_v T_a^2} \frac{p g_s}{g_s + g_a} \exp\left(\frac{\lambda}{R_v T_a^2} \frac{R_n^* - G^* + \frac{g_s g_a}{g_s + g_a} \rho \lambda q_a}{\rho c_p g_a / p} \right) \right)}{\lambda / (R_v T_a^2)} - \rho \lambda \frac{g_s g_a}{g_s + g_a} q_a$$
$$\to \frac{\rho c_p (g_g + g_r)}{\lambda / (R_v T_a^2)} W_0(0) - 0 = 0$$

since $W_0(0) = 0$. The key difference for the radiatively coupled case is that p varies with g_a, whereas in the radiatively uncoupled case, $p = 1$ and is invariant to changes in g_a.

Acknowledgments
Thanks to Pierre Gentine and Daniel Short Gianotti for providing feedback on a draft manuscript, Angela Rigden for assistance with processing the FLUXNET data, Changjie Lin for providing vegetation height information at each FLUXNET site, and Trevor Keenan for providing FLUXNET citations and site information via his FLUXNET_citations package on GitHub. This work was supported by funding from a Winokur Seed Grant in Environmental Sciences from the Harvard University Center for the Environment. The eddy covariance data used in this study can be accessed at https://daac.ornl.gov/cgi-bin/dataset_lister.pl?p=9. This work used eddy covariance data acquired and shared by the FLUXNET community, including these networks: AmeriFlux, AfriFlux, AsiaFlux, CarboAfrica, CarboEuropeIP, CarboItaly, CarboMont, ChinaFlux, Fluxnet-Canada, GreenGrass, ICOS, KoFlux, LBA, NECC, OzFlux-TERN, TCOS-Siberia, and USCCC. The ERA-Interim reanalysis data are provided by ECMWF and processed by LSCE. The FLUXNET eddy covariance data processing and harmonization was carried out by the European Fluxes Database Cluster, AmeriFlux Management Project, and Fluxdata project of FLUXNET, with the support of CDIAC and ICOS Ecosystem Thematic Center, and the OzFlux, ChinaFlux, and AsiaFlux offices.

References

Baldocchi, D. D., Krebs, T., & Leclerc, M. Y. (2005). "Wet/dry Daisyworld": A conceptual tool for quantifying the spatial scaling of heterogeneous landscapes and its impact on the subgrid variability of energy fluxes. *Tellus B: Chemical and Physical Meteorology*, *57*(3), 175–188. https://doi.org/10.3402/tellusb.v57i3.16538

Baldocchi, D. D., Luxmoore, R. J., & Hatfield, J. L. (1991). Discerning the forest from the trees: An essay on scaling canopy stomatal conductance. *Agricultural and Forest Meteorology*, *54*(2), 197–226. https://doi.org/10.1016/0168-1923(91)90006-C

Barr, A. G., Richardson, A. D., Hollinger, D. Y., Papale, D., Arain, M. A., Black, T. A., et al. (2013). Use of change-point detection for friction velocity threshold evaluation in eddy-covariance studies. *Agricultural and Forest Meteorology*, *171-172*, 31–45. https://doi.org/10.1016/j.agrformet.2012.11.023

Barry, D. A., Parlange, J. Y., Sander, G. C., & Sivaplan, M. (1993). A class of exact solutions for Richards' equation. *Journal of Hydrology*, *142*(1), 29–46. https://doi.org/10.1016/0022-1694(93)90003-R

Bateni, S. M., & Entekhabi, D. (2012). Relative efficiency of land surface energy balance components. *Water Resources Research*, *48*, W04510. https://doi.org/10.1029/2011WR011357/abstract

Corless, R. M., Gonnet, G. H., Hare, D. E. G., Jeffrey, D. J., & Knuth, D. E. (1996). On the Lambert *W* function. *Advances in Computational Mathematics*, *5*(1), 329–359. https://doi.org/10.1007/BF02124750

Dawson, T. E., Burgess, S. S. O., Tu, K. P., Oliveira, R. S., Santiago, L. S., Fisher, J. B., et al. (2007). Nighttime transpiration in woody plants from contrasting ecosystems. *Tree Physiology*, *27*(4), 561–575. https://doi.org/10.1093/treephys/27.4.561

De Kauwe, M. G., Medlyn, B. E., Knauer, J., & Williams, C. A. (2017). Ideas and perspectives: How coupled is the vegetation to the boundary layer? *Biogeosciences*, *14*(19), 4435–4453. https://doi.org/10.5194/bg-14-4435-2017

Fisher, J. B., Malhi, Y., Bonal, D., Rocha, H. R. D., Arajo, A. C. D., Gamo, M., et al. (2009). The land-atmosphere water flux in the tropics. *Global Change Biology*, *15*(11), 2694–2714. https://doi.org/10.1111/j.1365-2486.2008.01813.x

Fisher, J. B., Tu, K. P., & Baldocchi, D. D. (2008). Global estimates of the land-atmosphere water flux based on monthly AVHRR and ISLSCP-II data, validated at 16 FLUXNET sites. *Remote Sensing of Environment*, *112*(3), 901–919. https://doi.org/10.1016/j.rse.2007.06.025

Garratt, J. R. (1994). *The atmospheric boundary layer*. Cambridge: Cambridge University Press. Google-Books-ID: xeEVtBRApAkC.

Groh, J., Pütz, T., Gerke, H. H., Vanderborght, J., & Vereecken, H. (2019). Quantification and prediction of nighttime evapotranspiration for two distinct grassland ecosystems. *Water Resources Research*, *55*, 2961–2975. https://doi.org/10.1029/2018WR024072

Hamman, J. J., Nijssen, B., Bohn, T. J., Gergel, D. R., & Mao, Y. (2018). The Variable Infiltration Capacity model version 5 (VIC-5): Infrastructure improvements for new applications and reproducibility. *Geoscientific Model Development*, *11*(8), 3481–3496. https://doi.org/10.5194/gmd-11-3481-2018

Holtslag, A. a. M., & De Bruin, H. a. R. (1988). Applied modeling of the nighttime surface energy balance over land. *Journal of Applied Meteorology*, *27*(6), 689–704. https://doi.org/10.1175/1520-0450(1988)027<0689:AMOTNS>2.0.CO;2

Jarvis, P. G., & McNaughton, K. G. (1986). Stomatal control of transpiration: Scaling up from leaf to region. *Advances in Ecological Research*, *15*, 1–49. https://doi.org/10.1016/S0065-2504(08)60119-1

Jones, H. G. (2014). *Plants and microclimate: A quantitative approach to environmental plant physiology*. Cambridge: Cambridge University Press. Google-Books-ID: BYALAgAAQBAJ.

Konings, A. G., Dekker, S. C., Rietkerk, M., & Katul, G. G. (2011). Drought sensitivity of patterned vegetation determined by rainfall-land surface feedbacks. *Journal of Geophysical Research*, *116*, G04008. https://doi.org/10.1029/2011JG001748

Kumar, S. V., Wang, S., Mocko, D. M., Peters-Lidard, C. D., & Xia, Y. (2017). Similarity assessment of land surface model outputs in the North American Land Data Assimilation System. *Water Resources Research*, *53*, 8941–8965. https://doi.org/10.1002/2017WR020635

Lehtonen, J. (2016). The Lambert *W* function in ecological and evolutionary models. *Methods in Ecology and Evolution*, *7*(9), 1110–1118. https://doi.org/10.1111/2041-210X.12568

Liang, X., Lettenmaier, D. P., Wood, E. F., & Burges, S. J. (1994). A simple hydrologically based model of land surface water and energy fluxes for general circulation models. *Journal of Geophysical Research*, *99*(D7), 14,415–14,428. https://doi.org/10.1029/94JD00483

Lin, C., Gentine, P., Huang, Y., Guan, K., Kimm, H., & Zhou, S. (2018). Diel ecosystem conductance response to vapor pressure deficit is suboptimal and independent of soil moisture. *Agricultural and Forest Meteorology*, *250-251*, 24–34. https://doi.org/10.1016/j.agrformet.2017.12.078

Martens, B., Miralles, D. G., Lievens, H., van der Schalie, R., de Jeu, RichardA. M., Fernández-Prieto, D., et al. (2017). GLEAM v3: Satellite-based land evaporation and root-zone soil moisture. *Geoscientific Model Development*, *10*(5), 1903–1925. https://doi.org/10.5194/gmd-10-1903-2017

Martin, P. (1989). The significance of radiative coupling between vegetation and the atmosphere. *Agricultural and Forest Meteorology*, *49*(1), 45–53. https://doi.org/10.1016/0168-1923(89)90061-0

McColl, K. A., & Rigden, A. J. (2020). Emergent Simplicity of Continental Evapotranspiration. *Geophysical Research Letters 47*, e2020GL087101.

McColl, K. A., Salvucci, G. D., & Gentine, P. (2019). Surface flux equilibrium theory explains an empirical estimate of water-limited daily evapotranspiration. *Journal of Advances in Modeling Earth Systems*, *11*, 2036–2049. https://doi.org/10.1029/2019MS001685

McNaughton, K. (1976a). Evaporation and advection I: Evaporation from extensive homogeneous surfaces. *Quarterly Journal of the Royal Meteorological Society*, *102*(431), 181–191. https://doi.org/10.1002/qj.49710243115

McNaughton, K. G. (1976b). Evaporation and advection II: Evaporation downwind of a boundary separating regions having different surface resistances and available energies. *Quarterly Journal of the Royal Meteorological Society*, *102*(431), 193–202. https://doi.org/10.1002/qj.49710243116

McNaughton, K. G., & Jarvis, P. G. (1991). Effects of spatial scale on stomatal control of transpiration. *Agricultural and Forest Meteorology*, *54*(2-4), 279–302. https://doi.org/10.1016/0168-1923(91)90010-N

Medlyn, B. E., Kauwe, M. G. D., Lin, Y.-S., Knauer, J., Duursma, R. A., Williams, C. A., et al. (2017). How do leaf and ecosystem measures of water-use efficiency compare? *New Phytologist*, *216*(3), 758–770. https://doi.org/10.1111/nph.14626

Milly, P. C. D. (1991). A refinement of the combination equations for evaporation. *Surveys in Geophysics*, *12*(1), 145–154. https://doi.org/10.1007/BF01903416

Monteith, J. L. (1965). Evaporation and environment. In Fogg, G. E. (Ed.), *The state and movement of water in living organisms* (pp. 205–234). Cambridge, UK: Cambridge University Press.

Novick, K. A., Ficklin, D. L., Stoy, P. C., Williams, C. A., Bohrer, G., Oishi, A. C., et al. (2016). The increasing importance of atmospheric demand for ecosystem water and carbon fluxes. *Nature Climate Change*, *6*(11), 1023–1027. https://doi.org/10.1038/nclimate3114

10.1029/2020WR027106

Novick, K. A., Oren, R., Stoy, P. C., Siqueira, M. B. S., & Katul, G. G. (2009). Nocturnal evapotranspiration in eddy-covariance records from three co-located ecosystems in the Southeastern U.S.: Implications for annual fluxes. *Agricultural and Forest Meteorology*, *149*(9), 1491–1504. https://doi.org/10.1016/j.agrformet.2009.04.005

Papale, D., Reichstein, M., Aubinet, M., Canfora, E., Bernhofer, C., Kutsch, W., et al. (2006). Towards a standardized processing of Net Ecosystem Exchange measured with eddy covariance technique: Algorithms and uncertainty estimation. *Biogeosciences*, *3*(4), 571–583. https://doi.org/10.5194/bg-3-571-2006

Paulson, C. A. (1970). The mathematical representation of wind speed and temperature profiles in the unstable atmospheric surface layer. *Journal of Applied Meteorology*, *9*(6), 857–861. https://doi.org/10.1175/1520-0450(1970)009<0857:TMROWS>2.0.CO;2

Paw U, K. T., & Gao, W. (1988). Applications of solutions to non-linear energy budget equations. *Agricultural and Forest Meteorology*, *43*(2), 121–145. https://doi.org/10.1016/0168-1923(88)90087-1

Penman, H. L. (1948). Natural evaporation from open water, bare soil and grass. *Proceedings of the Royal Society of London. Series A. Mathematical and Physical Sciences*, *193*(1032), 120–145. https://doi.org/10.1098/rspa.1948.0037

Priestley, C. H. B., & Taylor, R. J. (1972). On the assessment of surface heat flux and evaporation using large-scale parameters. *Monthly Weather Review*, *100*(2), 81–92. https://doi.org/10.1175/1520-0493(1972)100<0081:OTAOSH>2.3.CO;2

Raupach, M. R. (2001). Combination theory and equilibrium evaporation. *Quarterly Journal of the Royal Meteorological Society*, *127*(574), 1149–1181.

Romps, D. M. (2016). Clausius-Clapeyron scaling of CAPE from analytical solutions to RCE. *Journal of the Atmospheric Sciences*, *73*(9), 3719–3737. https://doi.org/10.1175/JAS-D-15-0327.1

Romps, D. M. (2017). Exact expression for the lifting condensation level. *Journal of the Atmospheric Sciences*, *74*, 3891–3900. https://doi.org/10.1175/JAS-D-17-0102.1

Scheff, J., & Frierson, D. M. W. (2013). Scaling potential evapotranspiration with greenhouse warming. *Journal of Climate*, *27*(4), 1539–1558. https://doi.org/10.1175/JCLI-D-13-00233.1

Slatyer, R. O., & McIlroy, I. C. (1961). *Practical microclimatology: With special reference to the water factor in soil-plant-atmosphere relationships*. Melbourne, Australia: Commonwealth Scientific and Industrial Research Organisation English.

Stap, L. B., van den Hurk, B. J. J. M., van Heerwaarden, C. C., & Neggers, R. (2014). Modeled contrast in the response of the surface energy balance to heat waves for forest and grassland. *Journal of Hydrometeorology*, *15*(3), 973–989. https://doi.org/10.1175/JHM-D-13-029.1

Stavros, E. N., Schimel, D., Pavlick, R., Serbin, S., Swann, A., Duncanson, L., et al. (2017). ISS observations offer insights into plant function. *Nature Ecology & Evolution*, *1*, 0194. https://doi.org/10.1038/s41559-017-0194

Thom, A. S. (1975). Momentum, mass and heat exchange in plant communities. In J. L. Monteith (Ed.), *Vegetation and the atmosphere* (Vol. 1). London, UK: Academic Press.

Thom, A. S., & Oliver, H. R. (1977). On Penman's equation for estimating regional evaporation. *Quarterly Journal of the Royal Meteorological Society*, *103*(436), 345–357. https://doi.org/10.1002/qj.49710343610

Vallis, G. K., Parker, D. J., & Tobias, S. M. (2019). A simple system for moist convection: The rainy-Benard model. *Journal of Fluid Mechanics*, *862*, 162–199. https://doi.org/10.1017/jfm.2018.954

van Heerwaarden, C. C., Vil'a-Guerau de Arellano, J., Gounou, A., Guichard, F., & Couvreux, F. (2010). Understanding the daily cycle of evapotranspiration: A method to quantify the influence of forcings and feedbacks. *Journal of Hydrometeorology*, *11*(6), 1405–1422. https://doi.org/10.1175/2010JHM1272.1

Wullschleger, S. D., Gunderson, C. A., Hanson, P. J., Wilson, K. B., & Norby, R. J. (2002). Sensitivity of stomatal and canopy conductance to elevated CO_2 concentration interacting variables and perspectives of scale. *New Phytologist*, *153*(3), 485–496. https://doi.org/10.1046/j.0028-646X.2001.00333.x

Yang, Y., & Roderick, M. L. (2019). Radiation, surface temperature and evaporation over wet surfaces. *Quarterly Journal of the Royal Meteorological Society*, *1*(12). https://doi.org/10.1002/qj.3481

Yin, J., Albertson, J. D., Rigby, J. R., & Porporato, A. (2015). Land and atmospheric controls on initiation and intensity of moist convection: CAPE dynamics and LCL crossings. *Water Resources Research*, *51*, 8476–8493. https://doi.org/10.1002/2015WR017286

Supporting Information for "Practical and theoretical benefits of an alternative to the Penman-Monteith equation"

Kaighin A. McColl[1,2]

[1]Department of Earth and Planetary Sciences, Harvard University, Cambridge, MA 02138
[2]School of Engineering and Applied Sciences, Harvard University, Cambridge, MA 02138

Contents

Introduction

This document contains supporting text, figures and tables.

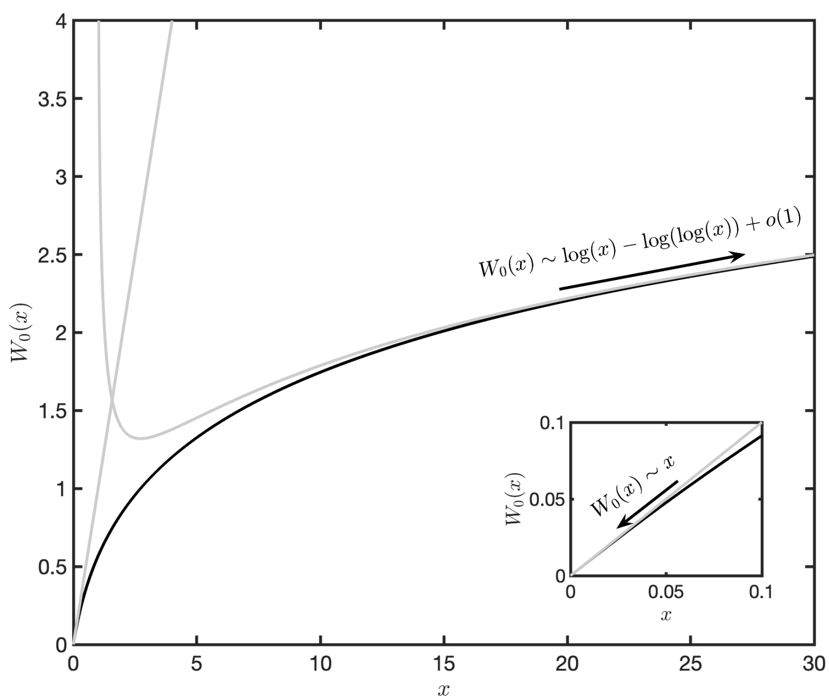

Figure S1. The principal branch of the Lambert-W function, $W_0(x)$ (black line), which asymptotically behaves as $W_0(x) \sim x$ as $x \to 0$, and $W_0(x) \sim \log(x) - \log(\log(x)) + o(1)$ as $x \to \infty$ (grey lines). Inset: zoomed in near $x = 0$.

Corresponding author: K.A. McColl, kmccoll@seas.harvard.edu

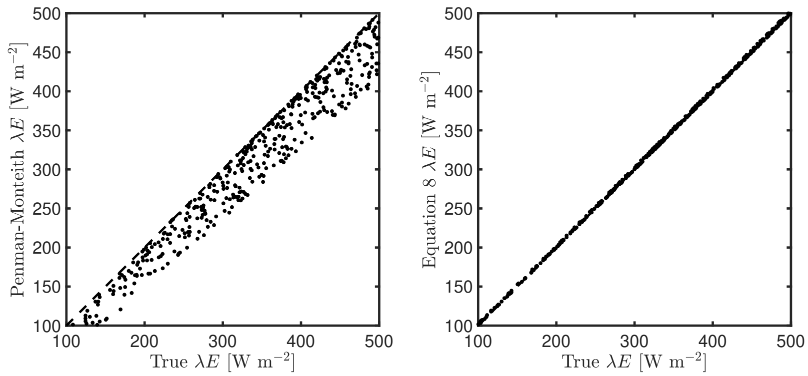

Figure S2. Left: Scatter plot comparing PM estimates of λE to true values, obtained by numerically solving equation 2, with $g_s = 10^{15}$ [m/s], RH = 0.5 [-], $T_a = 20$ [°C], P = 101,325 [Pa], $G = 0$ [W/m^2] and randomly varying g_a between 0.01 and 0.1 [m/s], and R_n between -200 and 500 [W/m^2]. Right: Same as left, but using equation 8, rather than the PM equation. In both plots, the axes are restricted to the range 100-500 [W m^{-2}] for visual clarity.

Text S1: Comparison of equation 8 and the PM equation using synthetic observations

The data used in section 2.1 are subject to observation errors. To address concerns that the results may be an artifact of errors in observations, or in modeled estimates of g_a, a synthetic analysis is presented in this section. Since no real data are used in this comparison, observation errors cannot impact the results.

Synthetic 'observations' of g_s, g_a, T_a, RH, and $R_n - G$ were generated by random sampling from uniform distributions, with ranges of $[10^{-4}, 0.03]$, $[0.01, 0.1]$, [253 K, 320 K], [0, 1], and $[-70 \text{ W/m}^2, 578 \text{ W/m}^2]$, respectively. The ranges of g_s, g_a and $R_n - G$ were chosen to correspond to the fifth and ninety-fifth percentiles of values estimated in the main text using real data. While these variables are often correlated in the real world, both the PM equation and equation 8 provide instantaneous estimates of λE; therefore, it is reasonable to test their accuracy when input variables are uncorrelated. The synthetic observations are used to estimate λE using both the PM equation and equation 8, and compared with the true value, obtained by numerically solving the surface energy budget (equation 1).

Figures S4a and b show the results of this analysis. Overall errors are substantially lower for equation 8 compared to the PM equation. They are also qualitatively consistent with the results obtained from the analysis using real data in the main text (Fig. 1).

Table S1: Site characteristics, studied periods, and citations for flux sites used in this analysis. All data obtained from www.fluxdata.org.

Site name	Veg[1]	Lat[2]	Lon[3]	Period	Ref[4]
AR-SLu	MF	-33.4648	-66.4598	2009-2011	*Ulke et al.* [2015]
AT-Neu	GRA	47.1167	11.3175	2002-2012	*Wohlfahrt et al.* [2008]
AU-ASM	ENF	-22.2830	133.2490	2010-2013	*Cleverly et al.* [2013]
AU-Cpr	SAV	-34.0021	140.5891	2010-2014	*Meyer et al.* [2015]
AU-DaP	GRA	-14.0633	131.3181	2007-2013	*Beringer et al.* [2011a]
AU-DaS	SAV	-14.1593	131.3881	2008-2014	*Hutley et al.* [2011]
AU-Dry	SAV	-15.2588	132.3706	2008-2014	*Cernusak et al.* [2011]
AU-Emr	GRA	-23.8587	148.4746	2011-2013	*Schroder et al.* [2014]
AU-Gin	WSA	-31.3764	115.7138	2011-2014	*Beringer et al.* [2016a]

Site name	Veg[1]	Lat[2]	Lon[3]	Period	Ref[4]
AU-How	WSA	-12.4943	131.1523	2001-2014	*Beringer et al.* [2007]
AU-Rig	GRA	-36.6499	145.5759	2011-2014	*Beringer et al.* [2016b]
AU-Stp	GRA	-17.1507	133.3502	2008-2014	*Beringer et al.* [2011b]
AU-Tum	EBF	-35.6566	148.1517	2001-2014	*Leuning et al.* [2005]
AU-Wac	EBF	-37.4259	145.1878	2005-2008	*Kilinc et al.* [2013]
AU-Whr	EBF	-36.6732	145.0294	2011-2014	*McHugh et al.* [2017]
AU-Wom	EBF	-37.4222	144.0944	2010-2012	*Hinko-Najera et al.* [2017]
AU-Ync	GRA	-34.9893	146.2907	2012-2014	*Yee et al.* [2015]
BE-Lon	CRO	50.5516	4.7461	2004-2014	*Moureaux et al.* [2006]
BE-Vie	MF	50.3051	5.9981	1996-2014	*Aubinet et al.* [2001]
BR-Sa3	EBF	-3.0180	-54.9714	2000-2004	*Wick et al.* [2005]
CA-Qfo	ENF	49.6925	-74.3421	2003-2010	*Bergeron et al.* [2007]
CA-SF1	ENF	54.4850	-105.8176	2003-2006	*Mkhabela et al.* [2009a]
CA-SF2	ENF	54.2539	-105.8775	2001-2005	*Mkhabela et al.* [2009b]
CH-Cha	GRA	47.2102	8.4104	2005-2014	*Merbold et al.* [2014]
CH-Dav	ENF	46.8153	9.8559	1997-2014	*Zielis et al.* [2014]
CH-Fru	GRA	47.1158	8.5378	2005-2014	*Imer et al.* [2013]
CN-Cng	GRA	44.5934	123.5092	2007-2010	*Dong* [2016]
DE-Geb	CRO	51.1001	10.9143	2001-2014	*Anthoni et al.* [2004]
DE-Gri	GRA	50.9500	13.5126	2004-2014	*Prescher et al.* [2010a]
DE-Hai	DBF	51.0792	10.4530	2000-2012	*Knohl et al.* [2003]
DE-Kli	CRO	50.8931	13.5224	2004-2014	*Prescher et al.* [2010b]
DE-Lkb	ENF	49.0996	13.3047	2009-2013	*Lindauer et al.* [2014]
DE-Obe	ENF	50.7867	13.7213	2008-2014	*Bernhofer et al.* [2016]
DE-Seh	CRO	50.8706	6.4497	2007-2010	*Schmidt et al.* [2012]
DE-Tha	ENF	50.9624	13.5652	1996-2014	*Grünwald and Bernhofer* [2007]
DK-Sor	DBF	55.4859	11.6446	1996-2014	*Pilegaard et al.* [2011]
FI-Hyy	ENF	61.8474	24.2948	1996-2014	*Suni et al.* [2003]
FI-Jok	CRO	60.8986	23.5135	2000-2003	*Lohila* [2004]
FI-Sod	ENF	67.3619	26.6378	2001-2014	*Thum et al.* [2007]
FR-Gri	CRO	48.8442	1.9519	2004-2013	*Loubet et al.* [2011]
FR-LBr	ENF	44.7171	-0.7693	1996-2008	*Berbigier et al.* [2001]
IT-CA2	CRO	42.3772	12.0260	2011-2014	*Sabbatini et al.* [2016]
IT-Col	DBF	41.8494	13.5881	1996-2014	*Valentini et al.* [1996]
IT-Cp2	EBF	41.7043	12.3573	2012-2014	*Fares et al.* [2014]
IT-Cpz	EBF	41.7052	12.3761	1997-2009	*Garbulsky et al.* [2008]
IT-Lav	ENF	45.9562	11.2813	2003-2014	*Marcolla et al.* [2003]
IT-MBo	GRA	46.0147	11.0458	2003-2013	*Marcolla et al.* [2011]
IT-Noe	CSH	40.6061	8.1515	2004-2014	*Papale et al.* [2014]
IT-PT1	DBF	45.2009	9.0610	2002-2004	*Migliavacca et al.* [2009]
IT-Ren	ENF	46.5869	11.4337	1998-2013	*Montagnani et al.* [2009]
IT-Ro2	DBF	42.3903	11.9209	2002-2012	*Tedeschi et al.* [2006]
IT-SRo	ENF	43.7279	10.2844	1999-2012	*Chiesi et al.* [2005]
IT-Tor	GRA	45.8444	7.5781	2008-2014	*Galvagno et al.* [2013]
NL-Hor	GRA	52.2404	5.0713	2004-2011	*Jacobs et al.* [2007]
NL-Loo	ENF	52.1666	5.7436	1996-2013	*Moors* [2012]
RU-Fyo	ENF	56.4615	32.9221	1998-2014	*Kurbatova et al.* [2008]
SD-Dem	SAV	13.2829	30.4783	2005-2009	*Ardo et al.* [2008]
US-AR1	GRA	36.4267	-99.4200	2009-2012	*Raz-Yaseef et al.* [2015a]
US-AR2	GRA	36.6358	-99.5975	2009-2012	*Raz-Yaseef et al.* [2015b]
US-ARM	CRO	36.6058	-97.4888	2003-2012	*Fischer et al.* [2007]
US-Blo	ENF	38.8953	-120.6328	1997-2007	*Goldstein et al.* [2000]
US-GLE	ENF	41.3665	-106.2399	2004-2014	*Frank et al.* [2014]
US-KS2	CSH	28.6086	-80.6715	2003-2006	*Powell et al.* [2006]

Site name	Veg[1]	Lat[2]	Lon[3]	Period	Ref[4]
US-Me2	ENF	44.4523	-121.5574	2002-2014	*Irvine et al.* [2008]
US-MMS	DBF	39.3232	-86.4131	1999-2014	*Dragoni et al.* [2011]
US-Ne1	CRO	41.1651	-96.4766	2001-2013	*Verma et al.* [2005a]
US-Ne2	CRO	41.1649	-96.4701	2001-2013	*Verma et al.* [2005b]
US-Ne3	CRO	41.1797	-96.4397	2001-2013	*Verma et al.* [2005c]
US-NR1	ENF	40.0329	-105.5464	1998-2014	*Monson et al.* [2002]
US-SRG	GRA	31.7894	-110.8277	2008-2014	*Scott et al.* [2015]
US-SRM	WSA	31.8214	-110.8661	2004-2014	*Scott et al.* [2009]
US-Syv	MF	46.2420	-89.3477	2001-2014	*Desai et al.* [2005]
US-Ton	WSA	38.4316	-120.9660	2001-2014	*Baldocchi et al.* [2010]
US-Var	GRA	38.4133	-120.9507	2000-2014	*Ma et al.* [2007]
US-WCr	DBF	45.8059	-90.0799	1999-2014	*Cook et al.* [2004]
US-Wkg	GRA	31.7365	-109.9419	2004-2014	*Scott et al.* [2010]
ZA-Kru	SAV	-25.0197	31.4969	2000-2010	*Archibald et al.* [2009]
ZM-Mon	DBF	-15.4378	23.2528	2000-2009	*Merbold et al.* [2009]

[1] Vegetation types: deciduous broadleaf forest (DBF); evergreen broadleaf forest (EBF); evergreen needleleaf forest (ENF); grassland (GRA); mixed deciduous and evergreen needleleaf forest (MF); savanna ecosystem (SAV); shrub ecosystem (SHR); wetland (WET); unknown (UNK). [2] Positive value indicates north latitude. [3] Negative value indicates west longitude. [4] References.

References

Anthoni, P. M., A. Knohl, C. Rebmann, A. Freibauer, M. Mund, W. Ziegler, O. Kolle, and E.-D. Schulze (2004), Forest and agricultural land-use-dependent CO2 exchange in Thuringia, Germany, *Global Change Biology*, *10*(12), 2005–2019, doi:10.1111/j.1365-2486.2004.00863.x.

Archibald, S. A., A. Kirton, M. R. van der Merwe, R. J. Scholes, C. A. Williams, and N. Hanan (2009), Drivers of inter-annual variability in net ecosystem exchange in a semi-arid savanna ecosystem, South Africa, *Biogeosciences*, *6*(2), 251–266, doi:10.5194/bg-6-251-2009.

Ardo, J., M. Molder, B. A. El-Tahir, and H. A. M. Elkhidir (2008), Seasonal variation of carbon fluxes in a sparse savanna in semi arid Sudan, *Carbon Balance and Management*, *3*(1), 7, doi:10.1186/1750-0680-3-7.

Aubinet, M., B. Chermanne, M. Vandenhaute, B. Longdoz, M. Yernaux, and E. Laitat (2001), Long term carbon dioxide exchange above a mixed forest in the Belgian Ardennes, *Agricultural and Forest Meteorology*, *108*(4), 293–315, doi:10.1016/s0168-1923(01)00244-1.

Baldocchi, D., Q. Chen, X. Chen, S. Ma, G. Miller, Y. Ryu, J. Xiao, R. Wenk, and J. Battles (2010), The dynamics of energy, water, and carbon fluxes in a blue oak (Quercus douglasii) savanna in California, in *Ecosystem Function in Savannas*, pp. 135–151, CRC Press, doi:10.1201/b10275-10.

Berbigier, P., J.-M. Bonnefond, and P. Mellmann (2001), CO2 and water vapour fluxes for 2 years above Euroflux forest site, *Agricultural and Forest Meteorology*, *108*(3), 183–197, doi:10.1016/s0168-1923(01)00240-4.

Bergeron, O., H. A. Margolis, T. A. Black, C. Coursolle, A. L. Dunn, A. G. Barr, and S. C. Wofsy (2007), Comparison of carbon dioxide fluxes over three boreal black spruce forests in Canada, *Global Change Biology*, *13*(1), 89–107, doi:10.1111/j.1365-2486.2006.01281.x.

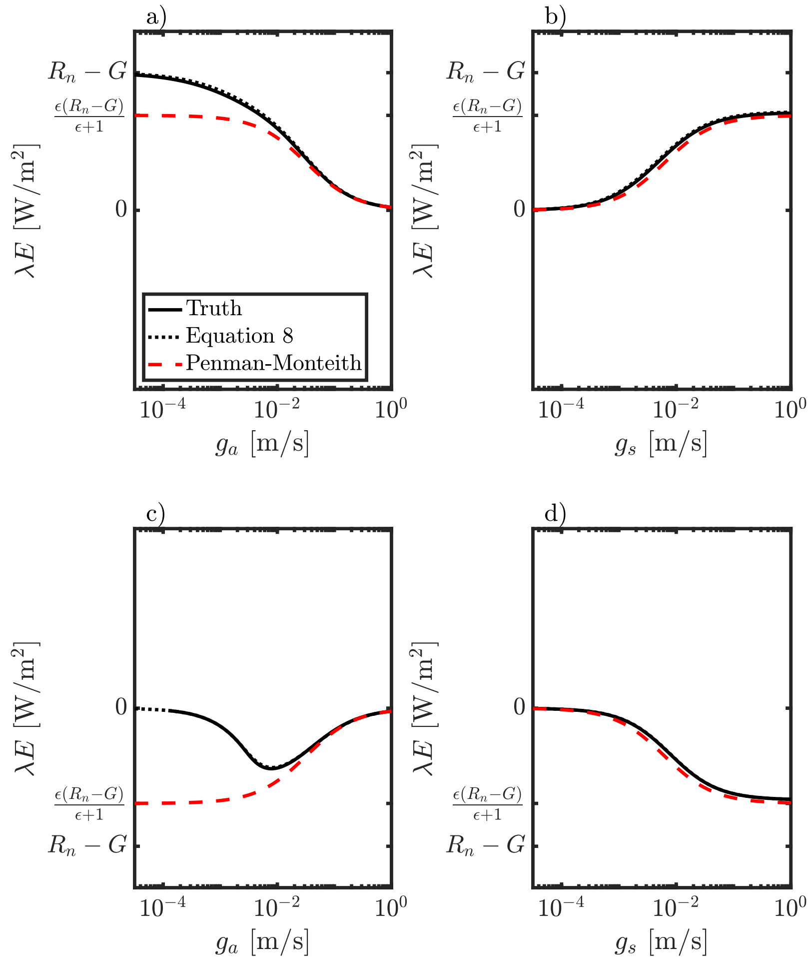

Figure S3. Variation of radiatively-uncoupled λE with changing aerodynamic conductance g_a (a, c) and surface conductance g_s (b, d), for $R_n - G > 0$ (a, b) and $R_n - G < 0$ (c, d). a) $g_s = 0.01$ [m/s], net radiation $R_n = 300$ [W/m^2], ground heat flux $G = 0$ [W/m^2], relative humidity $RH = 1$ [-], air pressure P = 101,325 [Pa], air temperature $T_a = 20$ [°C]. b) Same as a), except g_s varies and $g_a = 0.02$ [m/s]. c) Same as a), except $R_n = -300$ [W/m^2]. d) Same as b), except $R_n = -300$ [W/m^2].

Beringer, J., L. B. Hutley, N. J. Tapper, and L. A. Cernusak (2007), Savanna fires and their impact on net ecosystem productivity in North Australia, *Global Change Biology*, *13*(5), 990–1004, doi:10.1111/j.1365-2486.2007.01334.x.

Beringer, J., L. B. Hutley, J. M. Hacker, B. Neininger, and K. T. P. U (2011a), Patterns and processes of carbon, water and energy cycles across northern Australian landscapes: From point to region, *Agricultural and Forest Meteorology*, *151*(11), 1409–1416, doi: 10.1016/j.agrformet.2011.05.003.

Beringer, J., L. B. Hutley, J. M. Hacker, B. Neininger, and K. T. P. U (2011b), Patterns and processes of carbon, water and energy cycles across northern Australian landscapes: From point to region, *Agricultural and Forest Meteorology*, *151*(11), 1409–1416, doi: 10.1016/j.agrformet.2011.05.003.

Beringer, J., L. B. Hutley, I. McHugh, S. K. Arndt, D. Campbell, H. A. Cleugh, J. Cleverly, V. R. De Dios, D. Eamus, B. Evans, C. Ewenz, P. Grace, A. Griebel, V. Haverd, N. Hinko-Najera, A. Huete, P. Isaac, K. Kanniah, R. Leuning, M. J. Liddell, C. MacFarlane, W. Meyer, C. Moore, E. Pendall, A. Phillips, R. L. Phillips, S. M. Prober,

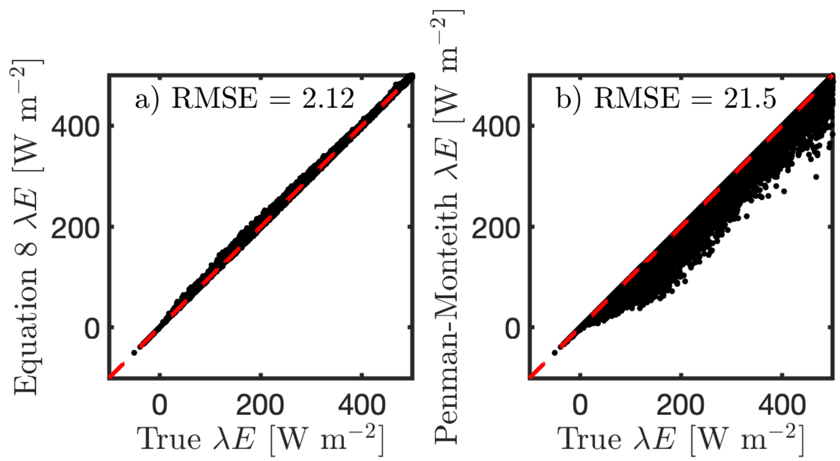

Figure S4. Comparison of a) equation 8 and b) the radiatively-uncoupled PM equation with synthetic observations, simulated as described in Text S1. The red dashed line is the 1:1 line. 'RMSE' means 'root-mean-squared error'.

N. Restrepo-Coupe, S. Rutledge, I. Schroder, R. Silberstein, P. Southall, M. Sun Yee, N. J. Tapper, E. Van Gorsel, C. Vote, J. Walker, and T. Wardlaw (2016a), An introduction to the Australian and New Zealand flux tower network - OzFlux, *Biogeosciences*, *13*(21), 5895–5916, doi:10.5194/bg-13-5895-2016.

Beringer, J., L. B. Hutley, I. McHugh, S. K. Arndt, D. Campbell, H. A. Cleugh, J. Cleverly, V. R. de Dios, D. Eamus, B. Evans, C. Ewenz, P. Grace, A. Griebel, V. Haverd, N. Hinko-Najera, A. Huete, P. Isaac, K. Kanniah, R. Leuning, M. J. Liddell, C. Macfarlane, W. Meyer, C. Moore, E. Pendall, A. Phillips, R. L. Phillips, S. M. Prober, N. Restrepo-Coupe, S. Rutledge, I. Schroder, R. Silberstein, P. Southall, M. S. Yee, N. J. Tapper, E. van Gorsel, C. Vote, J. Walker, and T. Wardlaw (2016b), An introduction to the Australian and New Zealand flux tower network – OzFlux, *Biogeosciences*, *13*(21), 5895–5916, doi:10.5194/bg-13-5895-2016.

Bernhofer, C., T. Grunwald, U. Moderow, M. Hehn, U. Eichelmann, and H. Prasse (2016), Fluxnet2015 de-obe oberbarenburg from 2008-2014, doi:10.18140/FLX/1440151.

Cernusak, L. A., L. B. Hutley, J. Beringer, J. A. Holtum, and B. L. Turner (2011), Photosynthetic physiology of eucalypts along a sub-continental rainfall gradient in northern Australia, *Agricultural and Forest Meteorology*, *151*(11), 1462–1470, doi: 10.1016/j.agrformet.2011.01.006.

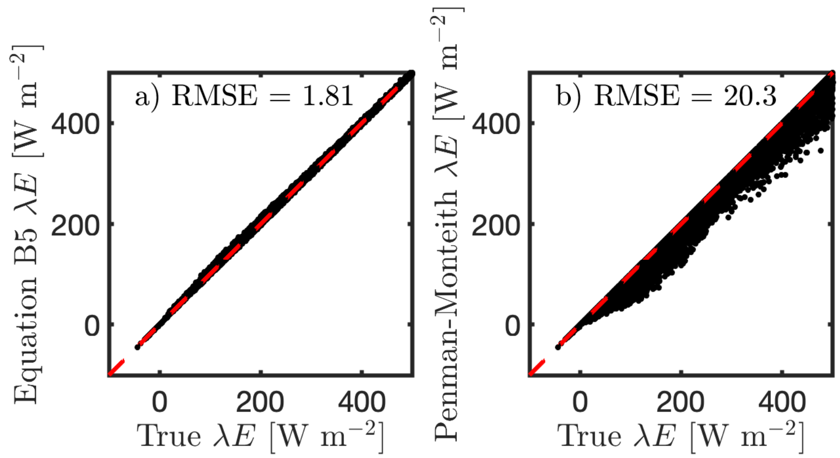

Figure S5. Same as Figure S4, but for the radiatively-coupled case, with $g_g = 0$ and $g_r = 4e_s\sigma T_a^3/(\rho c_p)$.

Chiesi, M., F. Maselli, M. Bindi, L. Fibbi, P. Cherubini, E. Arlotta, G. Tirone, G. Matteucci, and G. Seufert (2005), Modelling carbon budget of Mediterranean forests using ground and remote sensing measurements, *Agricultural and Forest Meteorology*, *135*(1-4), 22–34, doi:10.1016/j.agrformet.2005.09.011.

Cleverly, J., N. Boulain, R. Villalobos-Vega, N. Grant, R. Faux, C. Wood, P. G. Cook, Q. Yu, A. Leigh, and D. Eamus (2013), Dynamics of component carbon fluxes in a semi-arid Acacia woodland, central Australia, *Journal of Geophysical Research: Biogeosciences*, *118*(3), 1168–1185, doi:10.1002/jgrg.20101.

Cook, B. D., K. J. Davis, W. Wang, A. Desai, B. W. Berger, R. M. Teclaw, J. G. Martin, P. V. Bolstad, P. S. Bakwin, C. Yi, and W. Heilman (2004), Carbon exchange and venting anomalies in an upland deciduous forest in northern Wisconsin, USA, *Agricultural and Forest Meteorology*, *126*(3-4), 271–295, doi:10.1016/j.agrformet.2004.06.008.

Desai, A. R., P. V. Bolstad, B. D. Cook, K. J. Davis, and E. V. Carey (2005), Comparing net ecosystem exchange of carbon dioxide between an old-growth and mature forest in the upper Midwest, USA, *Agricultural and Forest Meteorology*, *128*(1-2), 33–55, doi:10.1016/j.agrformet.2004.09.005.

Dong, G. (2016), Fluxnet2015 cn-cng changling from 2007-2010, doi:10.18140/FLX/1440209.

Dragoni, D., H. P. Schmid, C. A. Wayson, H. Potter, C. S. B. Grimmond, and J. C. Randolph (2011), Evidence of increased net ecosystem productivity associated with a longer

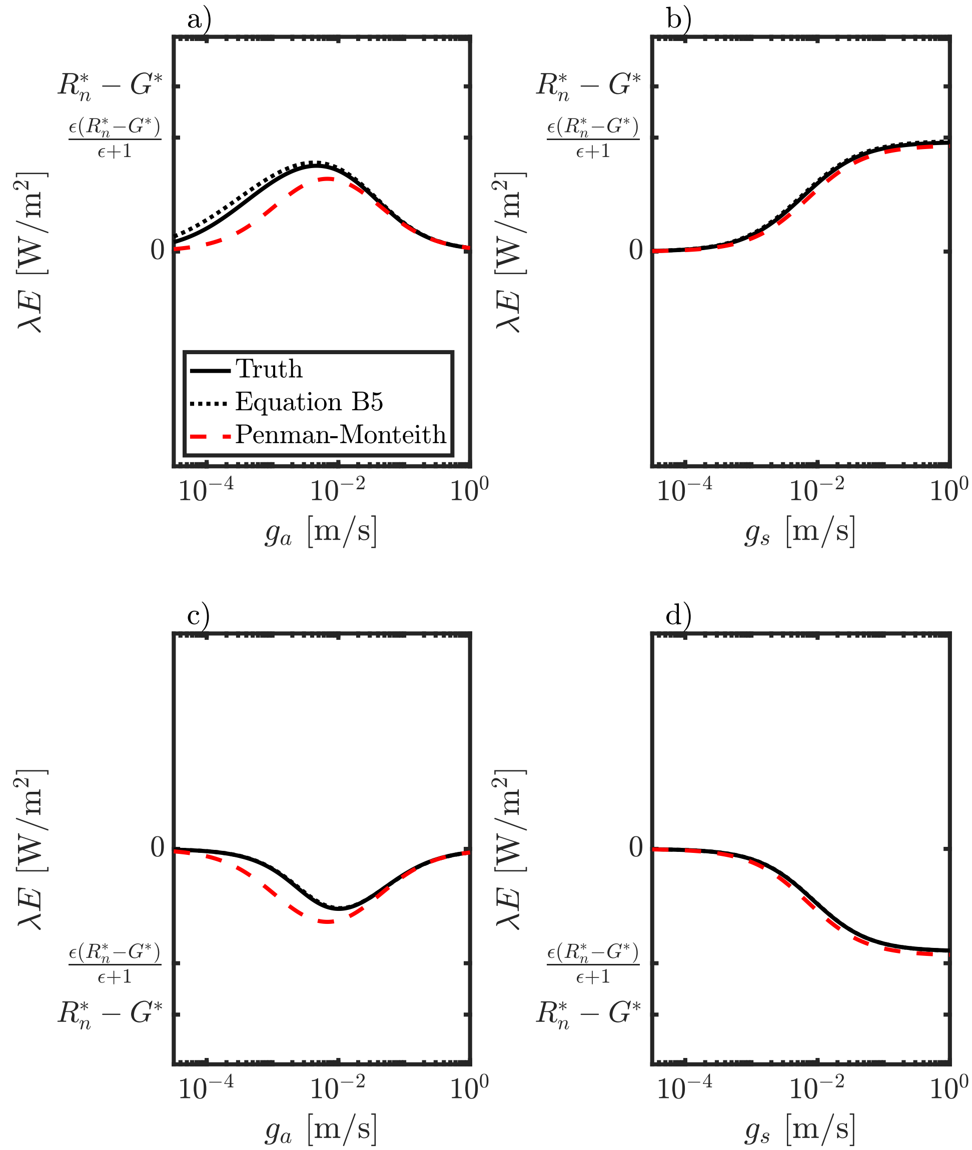

Figure S6. Same as Figure S3, but for the radiatively-coupled case, with $g_g = 0$ and $g_r = 4e_s\sigma T_a^3/(\rho c_p)$. See Appendix B for definition of terms.

vegetated season in a deciduous forest in south-central Indiana, USA, *Global Change Biology*, *17*(2), 886–897, doi:10.1111/j.1365-2486.2010.02281.x.

Fares, S., F. Savi, J. Muller, G. Matteucci, and E. Paoletti (2014), Simultaneous measurements of above and below canopy ozone fluxes help partitioning ozone deposition between its various sinks in a Mediterranean Oak Forest, *Agricultural and Forest Meteorology*, *198-199*, 181–191, doi:10.1016/j.agrformet.2014.08.014.

Fischer, M. L., D. P. Billesbach, J. A. Berry, W. J. Riley, and M. S. Torn (2007), Spatiotemporal variations in growing season exchanges of CO2, H2O, and sensible heat in agricultural fields of the southern Great Plains, *Earth Interactions*, *11*(17), 1–21, doi: 10.1175/ei231.1.

Frank, J. M., W. J. Massman, B. E. Ewers, L. S. Huckaby, and J. F. Negrón (2014), Ecosystem CO2/H2O fluxes are explained by hydraulically limited gas exchange during tree mortality from spruce bark beetles, *Journal of Geophysical Research: Biogeo-*

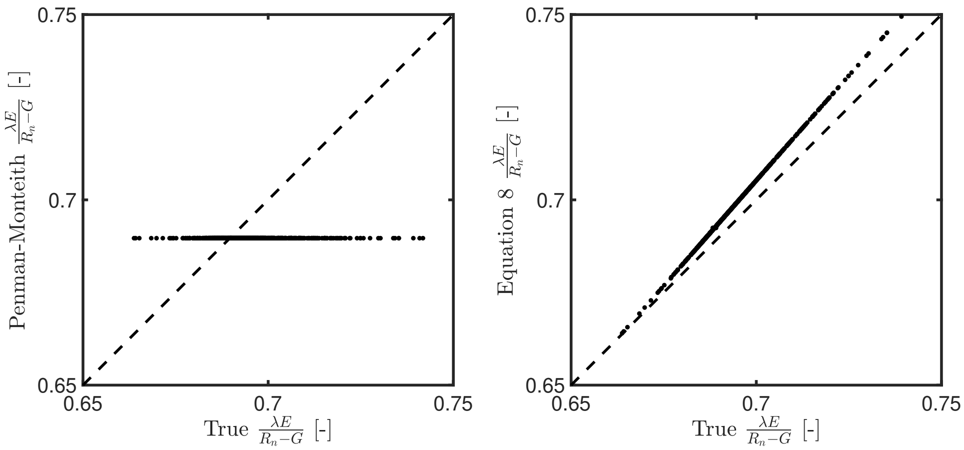

Figure S7. Left: Scatter plot comparing PM estimates of evaporative fraction to true values, obtained by numerically solving equation 2, with $g_s = 10^{15}$ [m/s], RH = 1 [-], $T_a = 20$ [°C], P = 101,325 [Pa], $G = 0$ [W/m^2] and randomly varying g_a between 0.01 and 0.1 [m/s], and R_n between -200 and 500 [W/m^2]. Right: Same as left, but using equation 8, rather than the PM equation.

sciences, *119*(6), 1195–1215, doi:10.1002/2013jg002597.

Galvagno, M., G. Wohlfahrt, E. Cremonese, M. Rossini, R. Colombo, G. Filippa, T. Julitta, G. Manca, C. Siniscalco, U. M. di Cella, and M. Migliavacca (2013), Phenology and carbon dioxide source/sink strength of a subalpine grassland in response to an exceptionally short snow season, *Environmental Research Letters*, *8*(2), 025,008, doi: 10.1088/1748-9326/8/2/025008.

Garbulsky, M. F., J. Peñuelas, D. Papale, and I. Filella (2008), Remote estimation of carbon dioxide uptake by a Mediterranean forest, *Global Change Biology*, *14*(12), 2860–2867, doi:10.1111/j.1365-2486.2008.01684.x.

Goldstein, A., N. Hultman, J. Fracheboud, M. Bauer, J. Panek, M. Xu, Y. Qi, A. Guenther, and W. Baugh (2000), Effects of climate variability on the carbon dioxide, water, and sensible heat fluxes above a ponderosa pine plantation in the Sierra Nevada (CA), *Agricultural and Forest Meteorology*, *101*(2-3), 113–129, doi:10.1016/s0168-1923(99)00168-9.

Grünwald, T., and C. Bernhofer (2007), A decade of carbon, water and energy flux measurements of an old spruce forest at the Anchor Station Tharandt, *Tellus B*, *59*(3), doi: 10.3402/tellusb.v59i3.17000.

Hinko-Najera, N., P. Isaac, J. Beringer, E. van Gorsel, C. Ewenz, I. McHugh, J.-F. Exbrayat, S. J. Livesley, and S. K. Arndt (2017), Net ecosystem carbon exchange of a dry temperate eucalypt forest, *Biogeosciences*, *14*(16), 3781–3800, doi:10.5194/bg-14-3781-2017.

Hutley, L. B., J. Beringer, P. R. Isaac, J. M. Hacker, and L. A. Cernusak (2011), A subcontinental scale living laboratory: Spatial patterns of savanna vegetation over a rainfall gradient in northern Australia, *Agricultural and Forest Meteorology*, *151*(11), 1417–1428, doi:10.1016/j.agrformet.2011.03.002.

Imer, D., L. Merbold, W. Eugster, and N. Buchmann (2013), Temporal and spatial variations of soil CO_2, CH_4 and N_2O fluxes at three differently managed grasslands, *Biogeosciences*, *10*(9), 5931–5945, doi:10.5194/bg-10-5931-2013.

Irvine, J., B. E. Law, J. G. Martin, and D. Vickers (2008), Interannual variation in soil CO2 efflux and the response of root respiration to climate and canopy gas exchange in mature ponderosa pine, *Global Change Biology*, *14*(12), 2848–2859, doi:10.1111/j.1365-2486.2008.01682.x.

Jacobs, C. M. J., A. F. G. Jacobs, F. C. Bosveld, D. M. D. Hendriks, A. Hensen, P. S. Kroon, E. J. Moors, L. Nol, A. Schrier-Uijl, and E. M. Veenendaal (2007), Variability of annual CO_2 exchange from Dutch grasslands, *Biogeosciences*, *4*(5), 803–816, doi:10.5194/bg-4-803-2007.

Kilinc, M., J. Beringer, L. B. Hutley, N. J. Tapper, and D. A. McGuire (2013), Carbon and water exchange of the world's tallest angiosperm forest, *Agricultural and Forest Meteorology*, *182-183*, 215–224, doi:10.1016/j.agrformet.2013.07.003.

Knohl, A., E.-D. Schulze, O. Kolle, and N. Buchmann (2003), Large carbon uptake by an unmanaged 250-year-old deciduous forest in central Germany, *Agricultural and Forest Meteorology*, *118*(3-4), 151–167, doi:10.1016/s0168-1923(03)00115-1.

Kurbatova, J., C. Li, A. Varlagin, X. Xiao, and N. Vygodskaya (2008), Modeling carbon dynamics in two adjacent spruce forests with different soil conditions in Russia, *Biogeosciences*, *5*(4), 969–980, doi:10.5194/bg-5-969-2008.

Leuning, R., H. A. Cleugh, S. J. Zegelin, and D. Hughes (2005), Carbon and water fluxes over a temperate eucalyptus forest and a tropical wet/dry savanna in Australia: measurements and comparison with MODIS remote sensing estimates, *Agricultural and Forest Meteorology*, *129*(3-4), 151–173, doi:10.1016/j.agrformet.2004.12.004.

Lindauer, M., H. Schmid, R. Grote, M. Mauder, R. Steinbrecher, and B. Wolpert (2014), Net ecosystem exchange over a non-cleared wind-throw-disturbed upland spruce forest—measurements and simulations, *Agricultural and Forest Meteorology*, *197*, 219–234, doi:10.1016/j.agrformet.2014.07.005.

Lohila, A. (2004), Annual CO2 exchange of a peat field growing spring barley or perennial forage grass, *Journal of Geophysical Research*, *109*(D18), doi:10.1029/2004jd004715.

Loubet, B., P. Laville, S. Lehuger, E. Larmanou, C. Fléchard, N. Mascher, S. Genermont, R. Roche, R. M. Ferrara, P. Stella, E. Personne, B. Durand, C. Decuq, D. Flura, S. Masson, O. Fanucci, J.-N. Rampon, J. Siemens, R. Kindler, B. Gabrielle, M. Schrumpf, and P. Cellier (2011), Carbon, nitrogen and greenhouse gases budgets over a four years crop rotation in northern France, *Plant and Soil*, *343*(1-2), 109–137, doi:10.1007/s11104-011-0751-9.

Ma, S., D. D. Baldocchi, L. Xu, and T. Hehn (2007), Inter-annual variability in carbon dioxide exchange of an oak/grass savanna and open grassland in California, *Agricultural and Forest Meteorology*, *147*(3-4), 157–171, doi:10.1016/j.agrformet.2007.07.008.

Marcolla, B., A. Pitacco, and A. Cescatti (2003), Canopy architecture and turbulence structure in a coniferous forest, *Boundary-Layer Meteorology*, *108*(1), 39–59, doi:10.1023/a:1023027709805.

Marcolla, B., A. Cescatti, G. Manca, R. Zorer, M. Cavagna, A. Fiora, D. Gianelle, M. Rodeghiero, M. Sottocornola, and R. Zampedri (2011), Climatic controls and ecosystem responses drive the inter-annual variability of the net ecosystem exchange of an alpine meadow, *Agricultural and Forest Meteorology*, *151*(9), 1233–1243, doi:10.1016/j.agrformet.2011.04.015.

McHugh, I. D., J. Beringer, S. C. Cunningham, P. J. Baker, T. R. Cavagnaro, R. M. Nally, and R. M. Thompson (2017), Interactions between nocturnal turbulent flux, storage and advection at an "ideal" eucalypt woodland site, *Biogeosciences*, *14*(12), 3027–3050, doi:10.5194/bg-14-3027-2017.

Merbold, L., J. Ardö, A. Arneth, R. J. Scholes, Y. Nouvellon, A. de Grandcourt, S. Archibald, J. M. Bonnefond, N. Boulain, N. Brueggemann, C. Bruemmer, B. Cappelaere, E. Ceschia, H. A. M. El-Khidir, B. A. El-Tahir, U. Falk, J. Lloyd, L. Kergoat, V. L. Dantec, E. Mougin, M. Muchinda, M. M. Mukelabai, D. Ramier, O. Roupsard, F. Timouk, E. M. Veenendaal, and W. L. Kutsch (2009), Precipitation as driver of carbon fluxes in 11 African ecosystems, *Biogeosciences*, *6*(6), 1027–1041, doi:10.5194/bg-6-1027-2009.

Merbold, L., W. Eugster, J. Stieger, M. Zahniser, D. Nelson, and N. Buchmann (2014), Greenhouse gas budget (CO2, CH4and N2O) of intensively managed grassland following restoration, *Global Change Biology*, *20*(6), 1913–1928, doi:10.1111/gcb.12518.

Meyer, W. S., E. Kondrlovà, and G. R. Koerber (2015), Evaporation of perennial semi-arid woodland in southeastern Australia is adapted for irregular but common dry periods, *Hydrological Processes*, *29*(17), 3714–3726, doi:10.1002/hyp.10467.

Migliavacca, M., M. Meroni, L. Busetto, R. Colombo, T. Zenone, G. Matteucci, G. Manca, and G. Seufert (2009), Modeling gross primary production of agro-forestry ecosystems by assimilation of satellite-derived information in a process-based model, *Sensors*, *9*(2), 922–942, doi:10.3390/s90200922.

Mkhabela, M., B. Amiro, A. Barr, T. Black, I. Hawthorne, J. Kidston, J. McCaughey, A. Orchansky, Z. Nesic, A. Sass, A. Shashkov, and T. Zha (2009a), Comparison of carbon dynamics and water use efficiency following fire and harvesting in Canadian boreal forests, *Agricultural and Forest Meteorology*, *149*(5), 783–794, doi:10.1016/j.agrformet.2008.10.025.

Mkhabela, M., B. Amiro, A. Barr, T. Black, I. Hawthorne, J. Kidston, J. McCaughey, A. Orchansky, Z. Nesic, A. Sass, A. Shashkov, and T. Zha (2009b), Comparison of carbon dynamics and water use efficiency following fire and harvesting in Canadian boreal forests, *Agricultural and Forest Meteorology*, *149*(5), 783–794, doi:10.1016/j.agrformet.2008.10.025.

Monson, R. K., A. A. Turnipseed, J. P. Sparks, P. C. Harley, L. E. Scott-Denton, K. Sparks, and T. E. Huxman (2002), Carbon sequestration in a high-elevation, subalpine forest, *Global Change Biology*, *8*(5), 459–478, doi:10.1046/j.1365-2486.2002.00480.x.

Montagnani, L., G. Manca, E. Canepa, E. Georgieva, M. Acosta, C. Feigenwinter, D. Janous, G. Kerschbaumer, A. Lindroth, L. Minach, S. Minerbi, M. Mölder, M. Pavelka, G. Seufert, M. Zeri, and W. Ziegler (2009), A new mass conservation approach to the study of CO2 advection in an alpine forest, *Journal of Geophysical Research*, *114*(D7), doi:10.1029/2008jd010650.

Moors, E. (2012), Water Use of Forests in The Netherlands, Ph.D. thesis, Vrije Universiteit Amsterdam.

Moureaux, C., A. Debacq, B. Bodson, B. Heinesch, and M. Aubinet (2006), Annual net ecosystem carbon exchange by a sugar beet crop, *Agricultural and Forest Meteorology*, *139*(1-2), 25–39, doi:10.1016/j.agrformet.2006.05.009.

Papale, D., M. Migliavacca, E. Cremonese, A. Cescatti, G. Alberti, M. Balzarolo, L. B. Marchesini, E. Canfora, R. Casa, P. Duce, O. Facini, M. Galvagno, L. Genesio, D. Gianelle, V. Magliulo, G. Matteucci, L. Montagnani, F. Petrella, A. Pitacco, G. Seufert, D. Spano, P. Stefani, F. P. Vaccari, and R. Valentini (2014), Carbon, water and energy fluxes of terrestrial ecosystems in Italy, in *The Greenhouse Gas Balance of Italy*, pp. 11–45, Springer Berlin Heidelberg, doi:10.1007/978-3-642-32424-6_2.

Pilegaard, K., A. Ibrom, M. S. Courtney, P. Hummelshøj, and N. O. Jensen (2011), Increasing net CO2 uptake by a Danish beech forest during the period from 1996 to 2009, *Agricultural and Forest Meteorology*, *151*(7), 934–946, doi:10.1016/j.agrformet.2011.02.013.

Powell, T. L., R. Bracho, J. Li, S. Dore, C. R. Hinkle, and B. G. Drake (2006), Environmental controls over net ecosystem carbon exchange of scrub oak in central Florida, *Agricultural and Forest Meteorology*, *141*(1), 19–34, doi:10.1016/j.agrformet.2006.09.002.

Prescher, A.-K., T. Grünwald, and C. Bernhofer (2010a), Land use regulates carbon budgets in eastern Germany: From NEE to NBP, *Agricultural and Forest Meteorology*, *150*(7-8), 1016–1025, doi:10.1016/j.agrformet.2010.03.008.

Prescher, A.-K., T. Grünwald, and C. Bernhofer (2010b), Land use regulates carbon budgets in eastern germany: From NEE to NBP, *Agricultural and Forest Meteorology*, *150*(7-8), 1016–1025, doi:10.1016/j.agrformet.2010.03.008.

Raz-Yaseef, N., D. P. Billesbach, M. L. Fischer, S. C. Biraud, S. A. Gunter, J. A. Bradford, and M. S. Torn (2015a), Vulnerability of crops and native grasses to summer drying in the U.S. southern Great Plains, *Agriculture, Ecosystems & Environment*, *213*, 209–218, doi:10.1016/j.agee.2015.07.021.

Raz-Yaseef, N., D. P. Billesbach, M. L. Fischer, S. C. Biraud, S. A. Gunter, J. A. Bradford, and M. S. Torn (2015b), Vulnerability of crops and native grasses to summer drying in the U.S. southern Great Plains, *Agriculture, Ecosystems & Environment*, *213*, 209–218, doi:10.1016/j.agee.2015.07.021.

Sabbatini, S., N. Arriga, T. Bertolini, S. Castaldi, T. Chiti, C. Consalvo, S. N. Djomo, B. Gioli, G. Matteucci, and D. Papale (2016), Greenhouse gas balance of cropland conversion to bioenergy poplar short-rotation coppice, *Biogeosciences*, *13*(1), 95–113, doi: 10.5194/bg-13-95-2016.

Schmidt, M., T. Reichenau, P. Fiener, and K. Schneider (2012), The carbon budget of a winter wheat field: An eddy covariance analysis of seasonal and inter-annual variability, *Agricultural and Forest Meteorology*, *165*, 114–126, doi:10.1016/j.agrformet.2012.05.012.

Schroder, I., T. Kuske, and S. Zegelin (2014), Eddy Covariance Dataset for Arcturus (2011-2013), Geoscience Australia, Canberra, *Tech. rep.*, doi:102.100.100/14249.

Scott, R. L., G. D. Jenerette, D. L. Potts, and T. E. Huxman (2009), Effects of seasonal drought on net carbon dioxide exchange from a woody-plant-encroached semiarid grassland, *Journal of Geophysical Research*, *114*(G4), doi:10.1029/2008jg000900.

Scott, R. L., E. P. Hamerlynck, G. D. Jenerette, M. S. Moran, and G. A. Barron-Gafford (2010), Carbon dioxide exchange in a semidesert grassland through drought-induced vegetation change, *Journal of Geophysical Research*, *115*(G3), doi:10.1029/2010jg001348.

Scott, R. L., J. A. Biederman, E. P. Hamerlynck, and G. A. Barron-Gafford (2015), The carbon balance pivot point of southwestern U.S. semiarid ecosystems: Insights from the 21st century drought, *Journal of Geophysical Research: Biogeosciences*, *120*(12), 2612–2624, doi:10.1002/2015jg003181.

Suni, T., J. Rinne, A. Reissel, N. Altimir, P. Keronen, Ü. Rannik, M. Maso, M. Kulmala, and T. Vesala (2003), Long-term measurements of surface fluxes above a Scots pine forest in Hyytiälä, southern Finland, *Boreal Environ. Res.*, *4*, 287–301.

Tedeschi, V., A. Rey, G. Manca, R. Valentini, P. G. Jarvis, and M. Borghetti (2006), Soil respiration in a Mediterranean oak forest at different developmental stages after coppicing, *Global Change Biology*, *12*(1), 110–121, doi:10.1111/j.1365-2486.2005.01081.x.

Thum, T., T. Aalto, T. Laurila, M. Aurela, P. Kolari, and P. Hari (2007), Parametrization of two photosynthesis models at the canopy scale in a northern boreal Scots pine forest, *Tellus B*, *59*(5), doi:10.3402/tellusb.v59i5.17066.

Ulke, A. G., N. N. Gattinoni, and G. Posse (2015), Analysis and modelling of turbulent fluxes in two different ecosystems in Argentina, *International Journal of Environment and Pollution*, *58*(1/2), 52, doi:10.1504/ijep.2015.076583.

Valentini, R., P. Angelis, G. Matteucci, R. Monaco, S. Dore, and G. E. S. Mucnozza (1996), Seasonal net carbon dioxide exchange of a beech forest with the atmosphere, *Global Change Biology*, *2*(3), 199–207, doi:10.1111/j.1365-2486.1996.tb00072.x.

Verma, S. B., A. Dobermann, K. G. Cassman, D. T. Walters, J. M. Knops, T. J. Arkebauer, A. E. Suyker, G. G. Burba, B. Amos, H. Yang, D. Ginting, K. G. Hubbard, A. A. Gitelson, and E. A. Walter-Shea (2005a), Annual carbon dioxide exchange in irrigated and rainfed maize-based agroecosystems, *Agricultural and Forest Meteorology*, *131*(1-2), 77–96, doi:10.1016/j.agrformet.2005.05.003.

Verma, S. B., A. Dobermann, K. G. Cassman, D. T. Walters, J. M. Knops, T. J. Arkebauer, A. E. Suyker, G. G. Burba, B. Amos, H. Yang, D. Ginting, K. G. Hubbard, A. A. Gitelson, and E. A. Walter-Shea (2005b), Annual carbon dioxide exchange in irrigated and rainfed maize-based agroecosystems, *Agricultural and Forest Meteorology*, *131*(1-2), 77–96, doi:10.1016/j.agrformet.2005.05.003.

Verma, S. B., A. Dobermann, K. G. Cassman, D. T. Walters, J. M. Knops, T. J. Arkebauer, A. E. Suyker, G. G. Burba, B. Amos, H. Yang, D. Ginting, K. G. Hubbard,

A. A. Gitelson, and E. A. Walter-Shea (2005c), Annual carbon dioxide exchange in irrigated and rainfed maize-based agroecosystems, *Agricultural and Forest Meteorology*, *131*(1-2), 77–96, doi:10.1016/j.agrformet.2005.05.003.

Wick, B., E. Veldkamp, W. Z. de Mello, M. Keller, and P. Crill (2005), Nitrous oxide fluxes and nitrogen cycling along a pasture chronosequence in central Amazonia, Brazil, *Biogeosciences*, *2*(2), 175–187, doi:10.5194/bg-2-175-2005.

Wohlfahrt, G., A. Hammerle, A. Haslwanter, M. Bahn, U. Tappeiner, and A. Cernusca (2008), Seasonal and inter-annual variability of the net ecosystem CO2 exchange of a temperate mountain grassland: Effects of weather and management, *Journal of Geophysical Research*, *113*(D8), doi:10.1029/2007jd009286.

Yee, M. S., V. R. Pauwels, E. Daly, J. Beringer, C. Rüdiger, M. F. McCabe, and J. P. Walker (2015), A comparison of optical and microwave scintillometers with eddy covariance derived surface heat fluxes, *Agricultural and Forest Meteorology*, *213*, 226–239, doi:10.1016/j.agrformet.2015.07.004.

Zielis, S., S. Etzold, R. Zweifel, W. Eugster, M. Haeni, and N. Buchmann (2014), NEP of a Swiss subalpine forest is significantly driven not only by current but also by previous year's weather, *Biogeosciences*, *11*(6), 1627–1635, doi:10.5194/bg-11-1627-2014.